



Transport pathways of peroxyacetyl nitrate

S. Fadnavis et al.

This discussion paper is/has been under review for the journal Atmospheric Chemistry and Physics (ACP). Please refer to the corresponding final paper in ACP if available.

Transport pathways of peroxyacetyl nitrate in the upper troposphere and lower stratosphere from different monsoon systems during the summer monsoon season

S. Fadnavis¹, K. Semeniuk², M. G. Schultz³, M. Kiefer⁴, A. Mahajan¹, L. Pozzoli⁵, and S. Sonbawane¹

¹Indian Institute of Tropical Meteorology, Pune, India

²Department of Earth and Space Sciences and Engineering, York University, Toronto, Canada

³Institute for Energy and Climate Research-Troposphere (IEK-8), Forschungszentrum Jülich, Jülich, Germany

⁴Karlsruhe Institute of Technology, Institute for Meteorology and Climate Research, Karlsruhe, Germany

⁵Eurasia Institute of Earth Sciences, Istanbul Technical University, Istanbul, Turkey

Title Page

Abstract

Introduction

Conclusions

References

Tables

Figures



Back

Close

Full Screen / Esc

Printer-friendly Version

Interactive Discussion



Received: 17 April 2015 – Accepted: 11 May 2015 – Published: 1 June 2015

Correspondence to: S. Fadnavis (suvarna@tropmet.res.in)

Published by Copernicus Publications on behalf of the European Geosciences Union.

ACPD

15, 15087–15135, 2015

Transport pathways of peroxyacetyl nitrate

S. Fadnavis et al.

Title Page

Abstract

Introduction

Conclusions

References

Tables

Figures



Back

Close

Full Screen / Esc

Printer-friendly Version

Interactive Discussion



Abstract

The Asian summer monsoon involves complex transport patterns with large scale re-distribution of trace gases in the upper troposphere and lower stratosphere (UTLS). We employ the global chemistry-climate model ECHAM5-HAMMOZ in order to evaluate the transport pathways and the contributions of nitrogen oxide species PAN, NO_x, and HNO₃ from various monsoon regions, to the UTLS over Southern Asia and vice versa. Simulated long term seasonal mean mixing ratios are compared with trace gas retrievals from the Michelson Interferometer for Passive Atmospheric Sounding aboard ENVISAT (MIPAS-E) and aircraft campaigns during the monsoon season (June–September) in order to evaluate the model's ability to reproduce these transport patterns.

The model simulations show that there are three regions which contribute substantial pollution to the South Asian UTLS: the Asian summer monsoon (ASM), the North American Monsoon (NAM) and the West African monsoon (WAM). However, penetration due to ASM convection reaches deeper into the UTLS as compared to NAM and WAM outflow. The circulation in all three monsoon regions distributes PAN into the tropical latitude belt in the upper troposphere. Remote transport also occurs in the extratropical upper troposphere where westerly winds drive North American and European pollutants eastward where they can become part of the ASM convection and be lifted into the lower stratosphere. In the lower stratosphere the injected pollutants are transported westward by easterly winds.

The intense convective activity in the monsoon regions is associated with lightning and thereby the formation of additional NO_x. This also affects the distribution of PAN in the UTLS. According to sensitivity simulations with and without lightning, increase in concentrations of PAN (~ 40 %), HNO₃ (75 %), NO_x (70 %) and ozone (30 %) over the regions of convective transport, especially over equatorial Africa and America and comparatively less over the ASM. This indicates that PAN in the UTLS over the ASM region is primarily of anthropogenic origin.

Transport pathways of peroxyacetyl nitrate

S. Fadnavis et al.

Title Page

Abstract

Introduction

Conclusions

References

Tables

Figures



Back

Close

Full Screen / Esc

Printer-friendly Version

Interactive Discussion



1 Introduction

Deep monsoon convection plays a key role in venting chemical constituents from the boundary layer and their export from source regions (Dickerson et al., 1987). The largest regional monsoon systems are the North American monsoon (NAM), Asian Summer Monsoon (ASM), Western North Pacific monsoon (WNPM), South American monsoon (SAM), West African Monsoon (WAM), and the Australian Monsoon (AUSM) (Chang et al., 2011). Recent observation and modeling studies indicate that the Asian summer monsoon (Park et al., 2004, 2007; Li et al., 2005; Randel and Park, 2006; Fu et al., 2006; Xiong et al., 2009; Randel et al., 2010; Fadnavis et al., 2013), the North American Monsoon (Schmitz and Mullen, 1996; Collier and Zhang, 2006; Barth et al., 2012) and the West African monsoon (Bouarar et al., 2011) play important roles in the transport of chemical constituents out of the boundary layer into the Northern Hemisphere subtropical monsoon anticyclone in the upper troposphere and lower stratosphere. However, until now there has been no attempt to assess the relative contributions from these source regions and to analyze the transport patterns including possible recirculation within one consistent model framework. Prior model simulations suggest that pollutants transported from the Asian monsoon region can contribute substantially to the budgets of stratospheric ozone, NO_x and water vapour (Randel et al., 2010). Ozone formation in the anticyclone is also enhanced by transport of pollution plumes from the North American monsoon which are rich in volatile organic compounds (VOC) (Li et al., 2005; Zhang et al., 2008; Choi et al., 2009; Barth et al., 2012). The deep monsoon convection over West Africa transports Central African emissions to the upper troposphere and lower stratosphere (UTLS) leading to large ozone changes in the lower stratosphere (Bouarar et al., 2011). A number of studies have reported transport of chemical constituents into the UTLS due to the Asian monsoon convection, while less attention has been paid to deep convective transport from North/South America and West Africa to the lower stratosphere and to their relative contributions to the UTLS composition over the ASM region.

Transport pathways of peroxyacetyl nitrate

S. Fadnavis et al.

Title Page

Abstract

Introduction

Conclusions

References

Tables

Figures



Back

Close

Full Screen / Esc

Printer-friendly Version

Interactive Discussion



**Transport pathways
of peroxyacetyl
nitrate**

S. Fadnavis et al.

Title Page

Abstract

Introduction

Conclusions

References

Tables

Figures



Back

Close

Full Screen / Esc

Printer-friendly Version

Interactive Discussion



This study investigates the transport patterns and relative contributions to the Asian monsoon anticyclone of three oxidized nitrogen species, namely peroxyacetyl nitrate (PAN), NO_x (the sum of NO and NO_2), and nitric acid (HNO_3). PAN is a secondary pollutant that marks the transport and conversion of surface NO_x after it is emitted. The focus is placed on PAN as this species has a long lifetime in the upper troposphere and can be favorably observed by satellite instruments. At the same time its short chemical lifetime in the lower troposphere results in a much tighter association between the emissions regions of its precursors and transport compared to species such as carbon monoxide (CO). The much longer chemical lifetime of CO in the lower troposphere allows it to reach the UTLS via circuitous pathways that are not accessible to PAN. In contrast, PAN is a tracer that allows for a clearer identification of NO_x pollution transport pathways between the surface and the UTLS.

PAN is formed through oxidation of non methane volatile organic compounds (NMVOCs) in the presence of NO_x (Fischer et al., 2014). It is primarily formed after oxidation of acetaldehyde (CH_3CHO) or after photolysis of acetone (CH_3COCH_3) and methyl glyoxal (CH_3COCHO), all of which are oxidation products of various NMVOCs. The actual formation of PAN proceeds in the reaction of the peroxy acetyl radical (CH_3CO_3) with NO_2 . This reaction is reversible and the thermal decomposition of PAN back to CH_3CO_3 and NO_2 is the main sink of PAN, although in the UTLS PAN photolysis becomes the dominant loss process. Two minor loss processes of PAN are reaction with OH and dry deposition (Talukdar et al., 1995; Fischer et al., 2014). As stated by Fischer et al. (2014) globally, biogenic VOC like isoprene and terpenes contribute most to PAN formation, but in the context of our study it is important to note that the oxidation of many alkanes and alkenes which are emitted from anthropogenic sources lead to PAN formation as well. The major anthropogenic sources of NMVOCs are the emissions from fossil fuel and biofuel combustion and from industrial solvents (Tang et al., 2009). Biomass burning, biogenic and soil emissions also contribute to NMVOC and NO_x production. Anthropogenic sources are dominant in the extra tropical Northern

Hemisphere outside the spring season. In spring, when surface PAN peaks, biogenic and anthropogenic NMVOCs species each support about 50 % of the PAN burden.

In the upper troposphere, lightning can add substantial amounts of NO_x and thus lead to additional PAN production if NMVOC precursors are present, e.g. from convective uplifting from the boundary layer (Tie et al., 2001). The estimated global NO_x production by lightning is $\sim 3\text{--}5 \text{ TgN year}^{-1}$ (Schumann and Huntrieser, 2007; Martin et al., 2007; Murray et al., 2012). Strong lightning activity during ASM, NAM and WAM (Shepon et al., 2007; Evett et al., 2008; Ranalkar and Chaudhari, 2009; Barret et al., 2010; Penki and Kamra, 2013) hence contributes to PAN production in the UTLS. The estimated increase in PAN is $\sim 20\text{--}30\%$ due to nitrogen enhancement by lightning (Tie et al., 2001).

The thermal decomposition rate of PAN is highly temperature dependent. In the UTLS temperatures are sufficiently low to prevent thermal decomposition of PAN and therefore the chemical lifetime of PAN in this region is several months (Arnold and Hauck, 1984). The PAN lifetime in our ECHAM5-HAMMOZ simulations varies between 80 and 170 days in the tropical UTLS (figure not included). Number of studies (Tereszchuk et al., 2013; Glatthor et al., 2007; Sign et al., 1987) has reported lifetime of PAN varying from 2–4 months. PAN therefore travels over long distances and affects the NO_y partitioning in areas that are far away from the precursor emission regions. Upon descent into warmer regions of the troposphere, PAN releases NO_x which in turn increases ozone and OH production in remote regions (Singh et al., 1986, 1998; Hudman et al., 2004). PAN mixing ratios vary from less than 1 pptv in the remote marine atmosphere (as observed during the NASA GTE PEM-Tropics B campaign in the South Pacific lower marine boundary layer, data available at <http://acd.ucar.edu/~emmons/DATACOMP/>) to several ppbv in the polluted urban environment and biomass burning plumes (Ridley et al., 1992; Singh et al., 1998). In the UTLS mixing ratios are typically in the range 10–300 pptv (Emmons et al., 2000; Keim et al., 2008).

Transport pathways of peroxyacetyl nitrate

S. Fadnavis et al.

Title Page

Abstract

Introduction

Conclusions

References

Tables

Figures



Back

Close

Full Screen / Esc

Printer-friendly Version

Interactive Discussion



**Transport pathways
of peroxyacetyl
nitrate**

S. Fadnavis et al.

Title Page

Abstract

Introduction

Conclusions

References

Tables

Figures



Back

Close

Full Screen / Esc

Printer-friendly Version

Interactive Discussion



To our knowledge, this is the first study that analyzes the influence of monsoon outflow from different world regions on the distribution of peroxyacetyl nitrate (PAN) in the UTLS over the Asian monsoon region, and its recirculation in the UTLS. We run decadal simulations with the chemistry climate model ECHAM5-HAMMOZ and apply statistical comparisons with satellite and aircraft data, thereby contributing to the objectives of the Chemistry Climate Model Initiative (CCMI, see <http://www.igacproject.org/CCMI>). The model climatology is evaluated with data from aircraft campaigns and the Michelson Interferometer for Passive Atmospheric Sounding (MIPAS) instrument onboard the ENVIRONMENTAL SATellite (ENVISAT) (Refereed as MIPAS-E hereafter). The transport of HNO₃ and NO_x due to monsoon convection from different monsoon regions and the impacts of lightning on the UTLS distributions of the nitrogen oxides are also analyzed and compared to the results obtained for PAN. The paper is organized as follows: Sect. 2 contains a short description of the data and model including the simulation setup. Comparison of model simulations with observations is given in Sect. 3. In Sect. 4, we discuss the various convective transport pathways of PAN into the UTLS, its redistribution in the stratosphere and its re-circulation across the various monsoon regions. The analysis of percentage changes in lightning produced ozone, HNO₃, PAN and NO_x on total concentrations over the convective zones is presented in Sect. 5. Conclusions are given in Sect. 6.

2 Methods

2.1 Satellite measurements

The MIPAS-E instrument onboard the ENVISAT was launched in March 2002 into a polar orbit of 800 km altitude, with an orbital period of about 100 min and an orbit repeat cycle of 35 days. MIPAS-E (Fischer and Oelhaf, 1996; Fischer et al., 2008) was a Fourier Transform Spectrometer that provided continual limb emission measurements in the mid infrared over the range 685–2410 cm⁻¹ (14.6–4.15 μm). From January 2005

through the end of the mission in April 2012 MIPAS was operated with a spectral resolution of 0.0875 cm^{-1} , and a stepping of the tangent altitude of 1.5–2 km in the UTLS region. As mid infrared sounder MIPAS-E could not provide spectral information from below cloud top.

MIPAS-E monitored several atmospheric trace constituents affecting atmospheric chemistry including PAN, NO_x , and O_3 . The details of the general retrieval method and setup, error estimates and use of averaging kernel and visibility flag are documented by Von Clarmann et al. (2009). In this study we analyze the MIPAS-E observed PAN data during the period 2005–2012, i.e. the data version V5R_PAN_220/V5R_PAN_221 (different naming 220/221 merely due to technical reasons). The data are available from http://share.lsd.fkit.edu/imk/asf/sat/mipas-export/Data_by_Target/. Details of the MIPAS PAN retrievals, error budget, and vertical resolution are given by Glatthor et al. (2007) and by Wiegele et al. (2012). Table 3 in Wiegele et al. (2012) indicates that for the total error of single profiles of the V5R_PAN_220/221 product the spectral noise and the uncertainty of the instrument pointing are the main contributors. However, since noise is a major contributor a reduction of the total error can be expected for vertical profiles of binned data. For typical bins used in this work the total errors are less than 10 % below 12 km, 30 % at 15 km, 50 % at 19 km and 80 % at 23 km.

The sensitivity of the PAN retrievals can be judged by the averaging kernels. For the V5R_PAN_220/221 product an example of the respective averaging kernel rows is shown in Fig. S1 for an altitude range of 5 to 25 km at 28° N and 85° E for cloud free atmospheric conditions. The diamonds indicate the respective nominal altitudes of the retrieval grid. The figure shows that the retrieval results below 8–9 km are dominated by information from above the nominal altitude. A similar, albeit less obvious, situation develops for altitudes above 22–23 km. There and above the information has an increasing weight from lower than nominal altitudes. This is the reason why the MIPAS PAN data is not considered below 8 km and above 23 km. Another effect clearly visible in the example is that the altitude region which influences the retrieved PAN value at a given altitude is increasing with altitude, i.e. the vertical resolution decreases with al-

Transport pathways of peroxyacetyl nitrate

S. Fadnavis et al.

Title Page

Abstract

Introduction

Conclusions

References

Tables

Figures



Back

Close

Full Screen / Esc

Printer-friendly Version

Interactive Discussion



titude. To account for the comparatively low, and altitude dependent, vertical resolution, the model data to be directly compared to MIPAS measurements was convolved with the MIPAS PAN averaging kernel.

The data are contoured and gridded at 4° latitude and 8° longitude resolution. In the process the data quality specifications as documented at <http://share.lsd.fkit.edu/imk/asf/sat/mipas-export/Documentation/> were employed, namely: only data with visibility flag equal 1 and diagonal value of averaging kernel greater than 0.03 were used.

2.2 ECHAM5-HAMMOZ model simulation and experimental setup

The ECHAM5-HAMMOZ aerosol-chemistry-climate model used in the present study comprises of the general circulation model ECHAM5 (Roeckner et al., 2003), the tropospheric chemistry module, MOZ (Horowitz et al., 2003), and the aerosol module, Hamburg Aerosol Model (HAM) (Stier et al., 2005). It includes ozone, NO_x, VOC and aerosol chemistry. The gas phase chemistry scheme is based on the MOZART-2 model (Horowitz et al., 2003), which includes comprehensive O_x-NO_x-hydrocarbons chemistry with 63 tracers and 168 reactions. The O(¹D) quenching reaction rates were updated according to Sander et al. (2003), and isoprene nitrates chemistry according to Fiore et al. (2005). In the model simulations we included emissions of acetone from anthropogenic sources and wild fires (primary sources), while acetaldehyde and methylglyoxal are produced by oxidation of other NMVOCs (secondary sources). In particular, oxidation of primary NMVOCs like ethane (C₂H₆), propane (C₃H₈) and propene (C₃H₆) forms acetaldehyde, while CH₃COCHO is mainly formed from the oxidation products of isoprene and terpenes. Higher acyl peroxy nitrates (MPAN) are included in MOZART-2 chemical scheme, they are also formed through oxidation of NMVOCs, but their production is small compared to PAN. Thermal decomposition, and reaction with OH as well as the absorption cross sections for PAN photolysis are all specified according to Sander et al. (2003).

In ECHAM5-HAMMOZ dry deposition follows the scheme of Ganzeveld and Lelieveld (1995). Soluble trace gases such as HNO₃ and SO₂ are also subject to wet depo-

Title Page

Abstract

Introduction

Conclusions

References

Tables

Figures



Back

Close

Full Screen / Esc

Printer-friendly Version

Interactive Discussion



sition. In-cloud and below cloud scavenging follows the scheme described by Stier et al. (2005). PAN is not water soluble, therefore dry and wet deposition are insignificant removal processes.

The model is run at a spectral resolution of T42 corresponding to about $2.8^\circ \times 2.8^\circ$ in the horizontal dimension and 31 vertical hybrid σ -p levels from the surface up to 10 hPa. We note that the nominal grid resolution of 2.8° is somewhat misleading, because the spectral truncation of T42 only allows to resolve details on the order of $180/42 = 4.28^\circ$. This is the main reason why we compare our model results with the MIPAS PAN retrievals on a $4^\circ \times 8^\circ$ grid. The details of model parameterizations, emissions and validation are described by Pozzoli et al., (2008a, b, 2011) and Fadnavis et al. (2013).

The simulations were performed with varying monthly mean sea surface temperature (SST) and sea ice cover (SIC) data over the period 1995–2004 (AMIP). The simulations did not aim to exactly reproduce specific meteorological years, and we ran 10 year periods in order to obtain a reasonable statistics. We used the RETRO project data set of the year 2000 available at <http://eccad.sedoo.fr/> for the surface CO, NO_x, and hydrocarbon emissions from anthropogenic sources and biomass burning (Schultz et al., 2004, 2007, 2008). Anthropogenic total RETRO emissions of the year 2000 are 476 Tg year⁻¹ for CO and 90 Tg year⁻¹ for NO_x, 5 Tg year⁻¹ of ethane, 3.5 Tg year⁻¹ of propane and 2.7 Tg year⁻¹ of propene, which are the main anthropogenic VOC precursors of PAN. Biomass burning RETRO emissions of year 2000 are 357 Tg year⁻¹ for CO, and 16 Tg year⁻¹ for NO_x. 2.5 Tg year⁻¹ for ethane, 1.3 Tg year⁻¹ for propane, 2.7 Tg year⁻¹ for propene, and 2.7 Tg year⁻¹ for acetone. CO biomass burning emissions in Southeast Asia account for 7 Gg month⁻¹ in spring, while up to 15 Gg month⁻¹ were reported from Carmichael et al. (2003). The anthropogenic and biomass burning emissions of SO₂ (total of 142 Tg year⁻¹), BC (7.7 Tg year⁻¹) and OC (66.1 Tg year⁻¹) are based on the AEROCOM emission inventory (Dentener et al., 2006), also representative of the year 2000. The biogenic NMVOC emissions are calculated on-line with the MEGAN module of Guenther et al. (2006). The simulated global annual mean emission of biogenic NMVOCs between 1995 and 2004 is 830 Tg(C) year⁻¹, isoprene

Transport pathways of peroxyacetyl nitrate

S. Fadnavis et al.

Title Page

Abstract

Introduction

Conclusions

References

Tables

Figures



Back

Close

Full Screen / Esc

Printer-friendly Version

Interactive Discussion



data sets and aircraft campaign used for comparison are presented in Table 1. For the comparison, aircraft observations are averaged over 0–2, 2–6 and 6–8 km and horizontally over the coherent flight regions.

2.3 Model production of PAN

PAN is a secondary pollutant that has a short lifetime in the lower troposphere. This reduces the number of source points that contribute to PAN concentrations at any location in the UTLS resulting in a clearer identification of source–receptor pathways. Figure 1 shows the distribution of PAN production at 14 and 16 km. A striking feature is the confinement of PAN production to regions of deep convection. A maximum daily production rate of PAN in the UTLS, in these convective zones, is $\sim 24 \text{ pptday}^{-1}$ (near 14 km). Production of PAN from background concentrations of ethane (C_2H_6) and other NMVOCs outside of deep convection regions is distinctly secondary. NMVOCs are subject to the same convective transport as NO_x and PAN formation occurs where both have the highest values. The lifetime of NO_x is short throughout the troposphere which implies that PAN production in the upper troposphere will be associated with deep convection. There is also a contribution to PAN production from stratospheric air penetrating into the troposphere (Liang et al., 2011). Tropopause folding is a significant source of exchange between the stratosphere and the troposphere (Gettelman et al., 2011). This is an extratropical process that is only likely to contribute to the PAN formation maxima over North America, Europe and Asia shown in Fig. 1a via enhanced conversion of ethane. In the model it is unable to obscure the relationship between PAN formation and NO_x pollution source regions.

Transport pathways of peroxyacetyl nitrate

S. Fadnavis et al.

Title Page

Abstract

Introduction

Conclusions

References

Tables

Figures



Back

Close

Full Screen / Esc

Printer-friendly Version

Interactive Discussion



3 Comparison of model simulations with observations

3.1 Comparison with aircraft measurements

Figure 2 shows scatter plot between aircraft observations and model simulations at the coherent locations. Both aircraft observations and model simulations are averaged for the monsoon season and altitude ranges. It indicates that model simulated PAN, O₃ and NO_x show good agreement with aircraft measurements. The Pearson's correlation coefficient (P value) varies between 0.00 to 0.4 indicating confidence level > 95%. However simulated HNO₃ between 2–6 and 6–10 km does not agree well with aircraft observations.

Figures showing the difference between ECHAM5-HAMMOZ and the aircraft observations are provided in the Supplement as Fig. S2. The model bias varies with species and altitude. Between 0–2 km (left column in Fig. S2), simulated PAN shows positive bias ~ 7–12 ppt in the Western Pacific, and 52–105 ppt over the United States of America (USA). Ozone exhibits a positive bias of ~ 7 ppb over India, ~ 2–18 ppb over the USA, ~ 3–15 ppb over western Pacific, negative biases between 2 and 20 ppb over the mid latitude Atlantic and a positive bias in the same range over the tropical Atlantic. Simulated HNO₃ is higher than the observations by ~ 20–75 ppt over the Western Pacific and by less than ~ -5 ppt at few locations. Over the USA the bias is slightly negative (less than 5 ppt). NO_x shows positive bias ~ 40 ppt over India and 0–10 ppt over the Western Pacific. In the altitude ranges 2–6 km (central column) and 6–10 km (right column), simulated PAN shows a negative bias of ~ 10–20 ppt over the West Pacific and a positive bias ~ 5–50 ppt at some locations. Over the USA bias values are ~ 4–70 ppt. Ozone is lower by ~ 10–15 ppb and higher by ~ 3–30 ppb at some locations in the western Pacific, 3–30 ppb over Atlantic and ~ 2–30 ppb over USA. The positive bias in HNO₃ reduces to 3–20 ppt and negative bias to 3 to 20 ppt over the Western Pacific, over the USA negative bias is ~ 20 ppt and positive bias is ~ 3–70 ppt. The NO_x shows negative bias ~ 40 ppt over India. The bias values vary between 6 to 10 ppt over Western Pacific, 15 to -20 ppt over USA and Atlantic. Thus, while ozone exhibits

a consistent low bias over South America and the Atlantic the model simulated ozone and NO_x mixing ratios show good agreement with CAIPEEX measurements over the Indian region. Unfortunately, there were no measurements of PAN or HNO_3 made during CAIPEEX.

3.2 Comparison with MIPAS-E retrievals

In order to study the influence of monsoon circulation on the distribution of PAN in the UTLS region, multi-year averages (2005–2011) of seasonal mean (June–September) PAN retrievals from MIPAS-E are analyzed. Figure 3a presents these data for the altitude range 14–16 km, and Fig. 3b shows the corresponding ECHAM5-HAMMOZ results for comparison. MIPAS-E observations show maximum PAN mixing ratios (~ 200 –230 ppt) over (1) the Asian monsoon anticyclone region (12 – 40° N, 20 – 120° E), and (2) over parts of North America, the Gulf Stream, (3) southern Atlantic Ocean and west coast of tropical Africa. ECHAM5-HAMMOZ CTRL simulations also show high PAN concentration at these locations, however PAN concentrations are lower than MIPAS-E observations and appear somewhat more localized. MIPAS-E exhibits a PAN maximum originating from African sources over the South Atlantic, whereas the model shows this maximum over the African continent. This may be the outflow of biomass burning over central and southern Africa during summer monsoon, which might be underestimated in the model. The biomass burning region of Africa during the ASM season is $\sim 30^\circ$ S– 20° N; 20° W– 30° E (Glanter et al., 2000). The longitude–altitude and latitude–altitude cross-sections of MIPAS-E observed and simulated PAN over the biomass burning region are plotted in Fig. S3. Model simulation shows that the biomass plume rising from Africa move westward and northward over the Atlantic Ocean and merges with South American plume. From satellite, aircraft observations and model simulations Real et al. (2010), and Barret et al. (2008) reported a plume in the mid and upper troposphere over the southern Atlantic which originates from central African biomass burning fires.

Transport pathways of peroxyacetyl nitrate

S. Fadnavis et al.

[Title Page](#)[Abstract](#)[Introduction](#)[Conclusions](#)[References](#)[Tables](#)[Figures](#)[Back](#)[Close](#)[Full Screen / Esc](#)[Printer-friendly Version](#)[Interactive Discussion](#)

**Transport pathways
of peroxyacetyl
nitrate**

S. Fadnavis et al.

Title Page

Abstract

Introduction

Conclusions

References

Tables

Figures



Back

Close

Full Screen / Esc

Printer-friendly Version

Interactive Discussion



The difference between ECHAM5-HAMMOZ simulation and MIPAS observations plotted in Fig. S3c and f. These figures show that the model underestimates biomass burning PAN by 20–60 ppt. These differences may also be related to issues in the vertical transport of PAN, or to a possible underestimate of the emission sources of NMVOCs. Uncertainties in the rate coefficients and absorption cross sections of PAN may also play a role. Furthermore, anthropogenic NO_x emissions are mostly underestimated in the emission inventories (Miyazaki et al., 2012). As discussed in Fadnavis et al. (2014), UTLS PAN over the ASM is sensitive to NO_x emission changes in India or China. In their study, also performed with ECHAM5-HAMMOZ, a 73 % NO_x emission change in India lead to a PAN increase of 10–18 %, while a 73 % NO_x emission change in China changed PAN over the ASM by 18–30 %. The cross-section plots of (see Fig. S4) differences in MIPAS-E PAN with model simulated PAN indicate that in the UTLS (8–23 km), MIPAS-E PAN is higher than model simulated PAN by ~ 20–60 ppt (except above 20 km). It is lower by 20–40 ppt over eastern part of anticyclone (Southern India and South east Asia) and also over Indonesia and northern Australia. In general, in the ASM region during the monsoon season MIPAS-E PAN is higher than model by 30–60 ppt between 8–16 km and the difference between MIPAS-E and model PAN vary between +40 to –40 ppt between 17 and 23 km.

4 Transport of PAN during monsoon season

4.1 Transport from Northern tropical land mass

Figure 3a shows high concentrations of PAN at 14–16 km over Asia, North America and tropical Africa. This may be due to transport from boundary layer into the UTLS by the monsoon convection from respective regions. From Satellite observations and model simulations Park et al. (2009) reported transport of fraction of boundary layer Carbon monoxide (CO) into the UTLS by the Asian monsoon convection.

To illustrate vertical transport, longitude–altitude cross sections of PAN mixing ratios averaged over the region 0–30° N and for June–September as obtained from MIPAS-E and ECHAM5-HAMMOZ are shown in Figs. 4a and b respectively. Both MIPAS-E observations and ECHAM5-HAMMOZ simulations show elevated levels of PAN (200–250 ppt) near 80–100° E (ASM), 30° W–30° E (WAM) and 80–100° W (NAM) region. The simulated PAN distribution along with winds plotted in Fig. 4b shows cross tropopause transport from these regions. It reveals that transport of boundary layer PAN to UTLS mainly occurs from strong convective regions, i.e. Bay of Bengal (~ 80–90° E), South China Sea (~ 100–120° E), western Atlantic Ocean (Gulf Stream region) and Gulf of Mexico (80–100° W). MIPAS-E observations and model simulations show that the transport due to ASM is strongest and reaches deepest into the lower stratosphere. This is due to the more intense deep convection activity over the ASM region compared to the NAM region. Over the ASM region the MIPAS-E observations show PAN mixing ratios of 30–60 ppt near 20 km while model simulations yield similar values near 22 km. Figure 4c presents the differences between MIPAS and model simulated PAN. It appears that the model PAN is overestimated over the ASM (20–50 ppt) and underestimated over the NAM (50–70 ppt) and WAM (20–70 ppt) regions. However, the overestimation in the upper troposphere in the ASM is difficult to explain on physical grounds and is more likely to be a MIPAS-E sampling issue as discussed later.

4.2 Transport from southern tropical land mass

In order to understand transport of PAN due to southern WAM, SAM and AUSM, we show longitude–pressure sections of MIPAS-E observations and model simulated PAN concentrations averaged over 0–25° S in Fig. 4d–e respectively. The model has plumes near 20° E, 100° E and 80° W. These three regions of convective transport are (1) tropical southern Africa 10–40° E, referred to as South Africa, (2) Indonesia and northern parts of Australia ~ 100–110° E and (3) South America ~ 70–80° W. Outflow from Indonesia and from northern parts of Australia (~ 100° E) penetrates deep into the UTLS. Tropical Rainfall Measuring Mission (TRMM) satellite observations show

Transport pathways of peroxyacetyl nitrate

S. Fadnavis et al.

Title Page

Abstract

Introduction

Conclusions

References

Tables

Figures



Back

Close

Full Screen / Esc

Printer-friendly Version

Interactive Discussion



**Transport pathways
of peroxyacetyl
nitrate**

S. Fadnavis et al.

Title Page

Abstract

Introduction

Conclusions

References

Tables

Figures



Back

Close

Full Screen / Esc

Printer-friendly Version

Interactive Discussion



high frequency of intense overshooting convection over these areas (during the monsoon season) with highest density in the belt 0–10° S over the Caribbean, Amazon, Congo and Southern Maritime Continent (Liu and Zipser, 2005). The analyses of vertical winds show strong transport from 10–40° E, 100–110° E, 70–80° W (in the belt 0–10° S). The amount of high level cloud fraction is also high over these regions. The model simulations show high PAN concentrations reaching the UTLS. Thus transport due to deep convection is reasonably well captured by the model. However, the MIPAS-E retrievals only show a plume rising over South Africa and no enhancement over the AUSM (Indonesia–Australia) and SAM regions. Figure 4e shows that the plumes from the three outflow regions are mixed in the upper troposphere (8–14 km) by the prevailing westerly winds. The reasons for a single plume seen in MIPAS-E may be that lower concentrations of PAN reach these altitudes (above 8 km) from SAM and AUSM and mix with the plume over South Africa. There are indications of elevated PAN concentrations at the lower boundary in Fig. 4d. Simulations show lower PAN mixing ratios over the longitudes of SAM and AUSM (see Fig. 4e). The differences between MIPAS observations and simulations (Fig. 4f) show that model PAN is overestimated in the AUSM (20–50 ppt) and is underestimated over the southern WAM (20–70 ppt) and SAM (20–60 ppt) regions. It is likely that the three plume structure in the upper troposphere seen in model is being obscured in the observations due to sampling issues since periods of deep convection reaching significantly above 8 km are associated with significant cloud cover.

Figure 4 shows that simulated transport of PAN due to ASM, NAM and WAM convection are stronger and penetrate deeper into the upper troposphere compared to SAM and AUSM. This is consistent with the distribution of deep convection noted by Gettelman et al. (2002). In general, the PAN amounts in the UTLS in the model are less than those observed by MIPAS-E. This may be due to an underestimate of the chemical PAN source from VOC precursors or too little vertical transport or a combination of both. Earlier model studies with ECHAM also exhibited too low concentrations of CO

get horizontally redistributed by the anticyclonic circulation and form the region of high PAN values between 40° N and high latitudes. Figure 9c shows that the mid-latitude maximum seen in Fig. 6c is due to pollution transport from Europe. The Chinese emissions are feeding into this large plume over Russia and are transported partly and diluted over the extratropical Pacific Ocean. The latitude–altitude section of differences between MIPAS and simulated PAN indicates that ASM plume is underestimated in the model (see Fig. 6c). It is interesting to compare Fig. 4c (longitude–altitude section) and Fig. 6c (latitude–altitude section). The reason for underestimation of the ASM plume in the latitude–altitude section may be due to a lower contribution from the eastern part of anticyclone in the model. Figure S4 shows model PAN is underestimated over Southern India and South East Asia in the upper troposphere and overestimated in the lower stratosphere. Figure 6c indicates that the region of convective transport in the model around 30° N is narrower than observations. The model also underestimates PAN in the upper troposphere around 45° N. It is possible that the model is not capturing the observed structure of the large scale ASM circulation and its northern limit in the UTLS. The overestimation of PAN by the model in the northern middle and high latitudes in the UTLS (Fig. 6c, f, i) is associated with European emissions and transport (see Fig. 6a, b, d, e, g, and h).

4.4 Transport from North American monsoon region

Figures 6d and e exhibit latitude–altitude sections of PAN from MIPAS-E retrievals and ECHAM5-HAMMOZ simulations (seasonal mean for July–September) over the North American monsoon region between 70–120° W. MIPAS-E observations and the model indicate transport of PAN into the UTLS. The distribution of ECHAM5-HAMMOZ simulated PAN from the boundary layer to UTLS shows the source region is at around 30° N. There is convective uplift of PAN over the northern Gulf of Mexico region and over the Gulf Stream. High amount of pollutants are emitted from north east America from a number of power plants are located in Atlanta, Washington, Chicago, Boston, Jacksonville (CEC report, 2011). The tropospheric NO₂ columns retrieved from the

Transport pathways of peroxyacetyl nitrate

S. Fadnavis et al.

Title Page

Abstract

Introduction

Conclusions

References

Tables

Figures



Back

Close

Full Screen / Esc

Printer-friendly Version

Interactive Discussion



PAN is underestimated over these regions (5–20° S and 20–40° N)). The reason may be related to underestimation of deep tropical convection in the model in this latitude band.

The model simulated latitude–altitude, longitude–altitude cross sections of NO_x , and HNO_3 over the ASM (10–40° N, 60–120° E), NAM (10–40° N, 70–120° W) and WAM (0–25° S, 0–45° E) are shown in Figs. 7 and 8, respectively. Figure 7 shows transport features of NO_x . These are similar to those seen in the distribution of PAN, but with sharper signatures due to the shorter lifetime of NO_x . This shows that monsoon convection lifts boundary layer pollutants including NO_y species to the UTLS. The distribution of HNO_3 (see Fig. 8) shows a complex pattern. Comparing Fig. 4b and c, the region around 100° E with intense convective uplift corresponds to HNO_3 depletion from the surface to above 10 km. In fact, the upper tropospheric region of the ASM anticyclone exhibits much lower values of HNO_3 compared to all the other longitudes in the 10–40° N band (Fig. 8c). This suggests that in the model the convective transport in the ASM region is associated with efficient removal by wet scavenging. In contrast, the North American monsoon region has HNO_3 ascending to the upper troposphere with significantly less loss. This is likely due to the fact that convection involved in vertical transport during the NAM is not as intense and not as deep as in the case of the ASM and there are differences in wet scavenging. Figure 8b shows that the plume rising from South America moves towards the equator but does not have the extension into the upper troposphere as the North American plume. These are June–September averages and the ITCZ is on the Northern Hemisphere side during this period. Thus, weaker convective transport is to be expected on the Southern Hemisphere side of the equator during this period. Figure 8d shows significant transport of African emissions around ~ 0–15° S and a plume rising from Europe (~ 35–60° N) as well.

4.6 Horizontal transport

PAN concentrations from MIPAS-E and ECHAM5-HAMMOZ at different altitudes are analyzed to understand horizontal transport. Figure 9a shows the distribution of PAN

**Transport pathways
of peroxyacetyl
nitrate**

S. Fadnavis et al.

Title Page

Abstract

Introduction

Conclusions

References

Tables

Figures



Back

Close

Full Screen / Esc

Printer-friendly Version

Interactive Discussion



layer pollution into the UTLS. Previous studies (e.g. Fadnavis et al., 2013) indicated that over the Asian monsoon region, transport into the lower stratosphere occurs and there is significant vertical transport over the southern slopes of the Himalayas (Fu et al., 2006; Fadnavis et al., 2013) and also over the region spanned by the Bay of Bengal and the South China Sea (Park et al., 2009). Pollutant transport due to North American convection and tropical African outflow does not penetrate as deep into the stratosphere as the ASM. However there is clear indication that in the upper troposphere, middle latitude westerly winds connect the North American pollution to the ASM.

Figures 3–6 and 9 show that in the upper troposphere, westerly winds drive North American and European pollutants eastward to at least partly merge with the ASM plume. Strong ASM convection transports these remote and regional pollutants into the stratosphere. The Caribbean is a secondary source of pollutant transport into the stratosphere. In the stratosphere the injected pollutants are transported westward by easterly winds and into the southern subtropics by the Brewer–Dobson circulation.

5 Impact of lightning on tropospheric PAN, NO_x, HNO₃ and ozone

In the ASM region and during the monsoon season the NO_x released from intense lightning activity enhances the formation of PAN, HNO₃ and ozone in the middle and upper troposphere which is already relatively strong due to the intense solar radiation along with high background concentrations of NO_x, HO_x and NMVOCs (Tie et al., 2001). Figure 10a–d shows the percentage changes in ozone, HNO₃, PAN and NO_x due to lightning as derived from the difference between the control and lightning-off experiments as zonally averaged spatial distribution of seasonal mean (June–September) mixing ratios. The analysis indicates that the impact of lightning on these species is largest in the tropical upper troposphere between 40° N–40° S and between 8 and 14 km. In the tropical mid troposphere lightning produced maximum ozone is ~ 15–25 % (12–24 ppb), HNO₃ ~ 40–60 % (50–90 ppt), PAN ~ 15–25 % (70–

140 ppt) and $\text{NO}_x \sim 20\text{--}40\%$ (10–35 ppt) while in the upper troposphere ozone is $\sim 20\text{--}30\%$ (20–28 ppb), $\text{HNO}_3 \sim 60\text{--}75\%$ (80–110 ppt), PAN $\sim 28\text{--}35\%$ (120–170 ppt), and $\text{NO}_x \sim 50\text{--}75\%$ (20–65 ppt). Our results are consistent with, albeit slightly lower than MOZART model simulations by Tie et al. (2001) who show that lightning enhances PAN formation by 20–30 %, $\text{NO}_x \sim 50\%$ and HNO_3 by 60–80 % in the middle troposphere. Labrador et al. (2005) also reported similar results from simulations using the Model of Atmospheric Transport and Chemistry Max-Planck-Institute (MATCH-MPI). The spatial distributions of NO_x , ozone, PAN and HNO_3 produced from lightning (see Fig. 10e–h) indicate that in the upper troposphere (12 km) increases in $\text{O}_3 \sim 20\text{--}25\%$ (11–17 ppbv), $\text{HNO}_3 \sim 40\text{--}70\%$, PAN $\sim 25\text{--}35\%$ and $\text{NO}_x \sim 55\text{--}75\%$, over North America are in agreement with previous studies (e.g Labrador et al., 2005; Hudman et al., 2007; Zhao et al., 2009; Cooper et al., 2009), over equatorial Africa (PAN 30–45 %, $\text{HNO}_3 \sim 70\text{--}80\%$, $\text{O}_3 \sim 25\%$, $\text{NO}_x \sim 70\%$) agrees well with Barret et al., 2010; Bouarar et al., 2011 and over the ASM region (PAN $\sim 25\%$, $\text{HNO}_3 \sim 65\text{--}70\%$, $\text{O}_3 \sim 20\%$, $\text{NO}_x \sim 60\text{--}70\%$) agrees with Tie et al. (2001). These regions coincide with regions of convective vertical transport of PAN (as seen in Figs. 4 and 6). PAN will be lifted into the lower stratosphere by the monsoon convection along with anthropogenic emissions and will redistribute in the tropical lower stratosphere. Latitude–longitude cross sections of lightning induced PAN, NO_x , ozone and HNO_3 formation at altitudes between 8–14 km show that the production of PAN, NO_x , ozone and HNO_3 is less over the ASM region than over the equatorial Americas and Africa (also seen in Fig. 10). The high amounts of PAN over the ASM (see Figs. 3, 4 and 6) are therefore primarily due to anthropogenic emission transport into the UTLS from the source regions in Southern and Eastern Asia. As discussed in Fadnavis et al., 2014, NO_x emissions are estimated to have changed by 38 % in India and 76 % in China, respectively during 2002–2011 period. From sensitivity simulations they deduced corresponding changes in upper tropospheric PAN are $> 40\%$, O_3 by $> 25\%$ and HNO_3 by $> 70\%$ over the Asian monsoon region. These effects are larger than the impact of lightning NO_x emissions over this region (Fig. 10e–h).

Transport pathways of peroxyacetyl nitrate

S. Fadnavis et al.

Title Page

Abstract

Introduction

Conclusions

References

Tables

Figures



Back

Close

Full Screen / Esc

Printer-friendly Version

Interactive Discussion



6 Conclusions

In this study statistical analysis of simulated and satellite-retrieved mixing ratios of PAN, NO_x , and HNO_3 is presented in order to determine the transport patterns of pollution into the Asian monsoon region and the impact of pollution flowing out of the ASM into other regions of the global atmosphere. The analysis focused on the upper troposphere and lower stratosphere and covered the period 2002–2011 without taking into account the emissions changes that occurred during this period. As discussed in Fadnavis et al. (2014), NO_x emissions are estimated to have changed by 38 % in India and 76 % in China, respectively during this period. From sensitivity simulations they deduced corresponding changes in upper tropospheric PAN > 40 %, O_3 by > 25 % and HNO_3 by > 70 % over the ASM region. These effects are larger than the impact of lightning NO_x emissions over this region discussed in Sect. 3 of this study.

Interestingly, the ECHAM5-HAMMOZ reveals that in the upper troposphere, westerly winds drive North American and northward propagating South African pollutants eastward where they mix with the ASM plume. Deep, overshooting convection and strong diabatic upwelling in the ASM, convectively transports a part of these plumes into the lower stratosphere. The Caribbean region is another source of pollution transport into the stratosphere. Some cross tropopause transport occurs due to overshooting convection over North America and Southern Africa as well. Some cross tropopause transport occurs due to overshooting convection over North America and Southern Africa as well. In the lower stratosphere the injected pollutants from ASM, WAM and NAM are transported westward by easterly winds and into the Southern Hemisphere subtropics by the Brewer–Dobson circulation. In the Southern Hemisphere, plumes rising from convective zones of South Africa, South America and Indonesia–Australia are evident in the model simulations, but are not seen in the MIPAS retrievals. PAN concentrations are higher in the plume rising from South Africa than SAM and AUSM. In the upper troposphere, they merge by the prevailing westerly winds. MIPAS-E observations in the UTLS show a single plume over South Africa and no enhancement over SAM or

Transport pathways of peroxyacetyl nitrate

S. Fadnavis et al.

Title Page

Abstract

Introduction

Conclusions

References

Tables

Figures



Back

Close

Full Screen / Esc

Printer-friendly Version

Interactive Discussion



**Transport pathways
of peroxyacetyl
nitrate**

S. Fadnavis et al.

Title Page

Abstract

Introduction

Conclusions

References

Tables

Figures



Back

Close

Full Screen / Esc

Printer-friendly Version

Interactive Discussion



AUSM. The reasons for the single plume seen in MIPAS-E may be that although there is uplifting by each of the three monsoon systems lower concentrations of PAN reach these altitudes (above 8 km) from SAM and AUSM until they merge with South African plume. It is also possible that the three plume structure in the upper troposphere seen in the model is being obscured in the observations due to sampling issues. Convective cloud cover is strongly associated with deep convection in the ASM region. The MIPAS-E data has a PAN minimum in the upper troposphere right in the longitude band of the deep convection over the southern flanks of the Himalayas (Fig. 4a). This feature is unphysical and clearly identifies a sampling bias. However, the model is also not fully reproducing the latitudinal structure of the PAN in the ASM region UTLS which indicates that there are differences in both the distribution of convection and the large scale circulation.

The horizontal transport of PAN analyzed from ECHAM5–HAMMOZ simulations shows that the PAN from southern Africa and Brazil is transported towards America by the circulation around a large upper-level anticyclone and then lifted to the UTLS in the NAM region.

The vertical distribution of simulated HNO_3 over the monsoon regimes shows low concentrations above 10 km at the foothills of the Himalayas. In contrast, the results show strong uplifting of HNO_3 into the upper troposphere with NAM convection. This may be due to the fact that NAM convection is not as intense as the ASM and there may be more wet removal of nitrogen oxides in the ASM convection. The model simulations indicate a higher efficiency of NO_x conversion to HNO_3 over the Indian region compared to NAM.

Lightning production of NO_x may enhance PAN concentrations in the upper troposphere and affect its transport into the lower stratosphere. The percentage change in lightning produced ozone, HNO_3 , PAN and NO_x has been evaluated with a sensitivity simulation. In the upper troposphere, lightning causes significant increases in these species over equatorial America, equatorial Africa and the ASM region. These regions coincide with intense convective zones with significant vertical transport. Lightning pro-

duction is higher over equatorial Africa and America compared to the ASM. However, the vertical distribution shows that higher amounts of PAN are transported into the upper troposphere in the ASM region. This indicates that the dominant contribution to PAN over the ASM is from anthropogenic emissions. This is consistent with the fact that anthropogenic emissions in the ASM region are higher than in the NAM and WAM (Lamsal et al., 2011; Miyazak et al., 2012).

Recent observations show a positive trend (with time) in lightning (Price and Asfur, 2006) and deep convective activity over the tropical land mass (Aumann and Ruzmaikin, 2013). TRMM precipitation radar also shows high density of deep overshooting events over the convective regions of the Caribbean, Mexico, Sahara desert, Congo and Indonesia (Liu and Zipser, 2005) during the summer monsoon season. This should amplify the UTLS trend from increasing tropospheric pollution. However, an analysis of this process is beyond the scope of this study.

**The Supplement related to this article is available online at
doi:10.5194/acpd-15-15087-2015-supplement.**

Acknowledgements. The authors thank the MIPAS-E teams for providing data and the High Power Computing Centre (HPC) in IITM, Pune, India, for providing computer resources.

References

Andreae, M. O., Artaxo, P., Fischer, H., Freitas, S. R., Grégoire, J.-M., Hansel, A., Hoor, P., Kormann, R., Krejci, R., Lange, L., Lelieveld, J., Lindinger, W., Longo, K., Peters, W., de Reus, M., Scheeren, B., Silva Dias, M. A. F., Ström, J., Velthoven, P. F. J., and van William, J.: Transport of biomass burning smoke to the upper troposphere by deep convection in the equatorial region, *Geophys. Res. Lett.*, 28, 951–958, 2001.

Transport pathways of peroxyacetyl nitrate

S. Fadnavis et al.

Title Page

Abstract

Introduction

Conclusions

References

Tables

Figures



Back

Close

Full Screen / Esc

Printer-friendly Version

Interactive Discussion



**Transport pathways
of peroxyacetyl
nitrate**

S. Fadnavis et al.

Title Page

Abstract

Introduction

Conclusions

References

Tables

Figures



Back

Close

Full Screen / Esc

Printer-friendly Version

Interactive Discussion



Arnold, F. and Hauck, G.: Lower stratosphere trace gas detection using aircraft-borne active chemical ionization mass spectrometry, *Nature*, 315, 307–309, doi:10.1038/315307a0, 1984.

Aumann, H. H. and Ruzmaikin, A.: Frequency of deep convective clouds in the tropical zone from 10 years of AIRS data, *Atmos. Chem. Phys.*, 13, 10795–10806, doi:10.5194/acp-13-10795-2013, 2013.

Barret, B., Ricaud, P., Mari, C., Attié, J.-L., Bousserrez, N., Josse, B., Le Flochmoën, E., Livesey, N. J., Massart, S., Peuch, V.-H., Piacentini, A., Sauvage, B., Thouret, V., and Cammas, J.-P.: Transport pathways of CO in the African upper troposphere during the monsoon season: a study based upon the assimilation of spaceborne observations, *Atmos. Chem. Phys.*, 8, 3231–3246, doi:10.5194/acp-8-3231-2008, 2008.

Barret, B., Williams, J. E., Bouarar, I., Yang, X., Josse, B., Law, K., Pham, M., Le Flochmoën, E., Liousse, C., Peuch, V. H., Carver, G. D., Pyle, J. A., Sauvage, B., van Velthoven, P., Schlager, H., Mari, C., and Cammas, J.-P.: Impact of West African Monsoon convective transport and lightning NO_x production upon the upper tropospheric composition: a multi-model study, *Atmos. Chem. Phys.*, 10, 5719–5738, doi:10.5194/acp-10-5719-2010, 2010.

Barth, M. C., Lee, J., Hodzic, A., Pfister, G., Skamarock, W. C., Worden, J., Wong, J., and Noone, D.: Thunderstorms and upper troposphere chemistry during the early stages of the 2006 North American Monsoon, *Atmos. Chem. Phys.*, 12, 11003–11026, doi:10.5194/acp-12-11003-2012, 2012.

Bouarar, I., Law, K. S., Pham, M., Liousse, C., Schlager, H., Hamburger, T., Reeves, C. E., Cammas, J.-P., Nédélec, P., Szopa, S., Ravegnani, F., Viciani, S., D'Amato, F., Ulanovsky, A., and Richter, A.: Emission sources contributing to tropospheric ozone over Equatorial Africa during the summer monsoon, *Atmos. Chem. Phys.*, 11, 13395–13419, doi:10.5194/acp-11-13395-2011, 2011.

Carmichael, G. R., Tang, Y., Kurata, G., Uno, I., Streets, D., Woo, J.-H., Huang, H., Yienger, J., Lefer, B., Shetter, R., Blake, D., Atlas, E., Fried, A., Apel, E., Eisele, F., Cantrell, C., Avery, M., Barrick, J., Sachse, G., Brune, W., Sandholm, S., Kondo, Y., Singh, H., Talbot, R., Bandy, A., Thornton, D., Clarke, A., and Heikes, B.: Regional-scale chemical transport modeling in support of the analysis of observations obtained during the TRACE-P experiment, *J. Geophys. Res.*, 108, 8823, doi:10.1029/2002JD003117, 2003.

CEC (Commission for Environmental Cooperation): Report on North American Power Plant Air Emissions, Montréal (Québec) Canada, ISBN: 978–2-89700–008-0, 2011.

Transport pathways of peroxyacetyl nitrate

S. Fadnavis et al.

Title Page

Abstract

Introduction

Conclusions

References

Tables

Figures



Back

Close

Full Screen / Esc

Printer-friendly Version

Interactive Discussion



Chang, C.-P., Ding, Y., Lau, G. N.-C., Johnson, R. H., Wang, B., and Yasunari, T. (Eds.): The Global Monsoon System: Research and Forecast (2nd Edn.), World Scientific Publishing Co., 2011.

Choi, Y., Kim, J., Eldering, A., Osterman, G., Yung, Y. L., Gu, Y., and Liou, K. N.: Light-
5 ning and anthropogenic NO_x sources over the United States and the western North Atlantic Ocean: impact on OLR and radiative effects, *Geophys. Res. Lett.*, 36, L17806, doi:10.1029/2009GL039381, 2009.

Collier, J. C. and Zhang, G. J.: Simulation of the North American Monsoon by the NCAR CCM3 and its sensitivity to convection parameterization, *J. Climate*, 19, 2851–2866, 2006.

10 Cooper, O. R., Eckhardt, S., Crawford, J. H., Brown, C. C., Cohen, R. C., Bertram, T. H., Wooldridge, P., Perring, A., Brune, W. H., Ren, X., Brunner, D., and Baughcum, S. L.: Summertime buildup and decay of lightning NO_x and aged thunderstorm outflow above North America, *J. Geophys. Res.*, 114, D01101, doi:10.1029/2008JD010293, 2009.

Dickerson, R. R., Huffman, G. J., Luke, W. T., Nunnermacker, L. J., Pickering, K. E., Leslie, A., Lindsey, C., Slinn, W., Kelly, T., Daum, P., Delany, A., Grennberg, J., Zimmerman, P., Boatman, J., Ray, J., and Stedman, D.: Thunderstorms: an important mechanism in the transport of air pollutants, *Science*, 235, 460–465, 1987.

Dong, L. and Colucci, S. J.: The role of deformation and potential vorticity in Southern Hemisphere blocking onsets, *J. Atmos. Sci.*, 62, 4043–4056, 2005.

20 Drummond, J. W., Ehhalt, D. H., and Volz, A.: Measurements of nitric oxide between 0–12 km altitude and 67N–60S latitude obtained during STRATOZ III, *J. Geophys. Res.*, 93, 15831–15849, 1988.

Emmons, L. K., Hauglustaine, D. A., Muller, J.-F., Carroll, M. A., Brasseur, G. P., Brunner, D., Staehelin, J., Thouret, V., and Marenco, A.: Data composites of tropospheric ozone and its precursors from aircraft measurements, *J. Geophys. Res.*, 105, 20497–20538, 2000.

25 Evett, R. R., Mohrle, C. R., Hall, B. L., Brown, T. J., and Stephens, S. L.: The effect of monsoonal atmospheric moisture on lightning fire ignitions in southwestern North America, *Agr. Forest Meteorol.*, 148, 1478–1487, 2008.

Fadnavis, S., Semeniuk, K., Pozzoli, L., Schultz, M. G., Ghude, S. D., Das, S., and Kakatkar, R.: Transport of aerosols into the UTLS and their impact on the Asian monsoon region as seen in a global model simulation, *Atmos. Chem. Phys.*, 13, 8771–8786, doi:10.5194/acp-13-8771-2013, 2013.

**Transport pathways
of peroxyacetyl
nitrate**

S. Fadnavis et al.

Title Page

Abstract

Introduction

Conclusions

References

Tables

Figures



Back

Close

Full Screen / Esc

Printer-friendly Version

Interactive Discussion



Fadnavis, S., Schultz, M. G., Semeniuk, K., Mahajan, A. S., Pozzoli, L., Sonbawane, S., Ghude, S. D., Kiefer, M., and Eckert, E.: Trends in Peroxyacetyl Nitrate (PAN) in the upper troposphere and lower stratosphere over Southern Asia during the summer monsoon season: regional impacts, *Atmos. Chem. Phys. Discuss.*, 14, 19055–19094, doi:10.5194/acpd-14-19055-2014, 2014.

Fiore, A. M., Horowitz, L. W., Purves, D. W., Levy II, H., Evans, M. J., Wang, Y., Li, Q., and Yantosca, R. M.: Evaluating the contribution of changes in isoprene emissions to surface ozone trends over the eastern United States, *J. Geophys. Res.*, 110, D12303, doi:10.1029/2004JD005485, 2005.

Fischer, E. V., Jacob, D. J., Yantosca, R. M., Sulprizio, M. P., Millet, D. B., Mao, J., Paulot, F., Singh, H. B., Roiger, A., Ries, L., Talbot, R. W., Dzepina, K., and Pandey Deolal, S.: Atmospheric peroxyacetyl nitrate (PAN): a global budget and source attribution, *Atmos. Chem. Phys.*, 14, 2679–2698, doi:10.5194/acp-14-2679-2014, 2014.

Fischer, H. and Oelhaf, H.: Remote sensing of vertical profiles of atmospheric trace constituents with MIPAS limb-emission spectrometers, *Appl. Optics*, 35, 2787–2796, 1996.

Fischer, H., Birk, M., Blom, C., Carli, B., Carlotti, M., von Clarmann, T., Delbouille, L., Dudhia, A., Ehhalt, D., Endemann, M., Flaud, J. M., Gessner, R., Kleinert, A., Koopman, R., Langen, J., López-Puertas, M., Mosner, P., Nett, H., Oelhaf, H., Perron, G., Remedios, J., Ridolfi, M., Stiller, G., and Zander, R.: MIPAS: an instrument for atmospheric and climate research, *Atmos. Chem. Phys.*, 8, 2151–2188, doi:10.5194/acp-8-2151-2008, 2008.

Fu, R., Hu, Y., Wright, J. S., Jiang, J. H., Dickinson, R. E., Chen, M., Filipiak, M., Read, W. G., Waters, J. W., and Wu, D. L.: Short circuit of water vapour and polluted air to the global stratosphere by convective transport over the Tibetan Plateau, *P. Natl. Acad. Sci. USA*, 103, 5664–5669, 2006.

Galanter, M., Levy II, H., and Carmichael, G. R.: Impacts of biomass burning on tropospheric CO, NO_x, and O₃, *J. Geophys. Res.*, 105, 6633–6653, doi:10.1029/1999JD901113, 2000.

Ganzeveld, L. and Lelieveld, J.: Dry deposition parameterization in a chemistry general circulation model and its influence on the distribution of reactive trace gases, *J. Geophys. Res.*, 100, 20999–21012, doi:10.1029/95JD02266, 1995.

Garny, H. and Randel, W. J.: Dynamic variability of the Asian monsoon anticyclone observed in potential vorticity and correlations with tracer distributions, *J. Geophys. Res.-Atmos.*, 118, 13421–13433, doi:10.1002/2013JD020908, 2013.

**Transport pathways
of peroxyacetyl
nitrate**

S. Fadnavis et al.

Title Page

Abstract

Introduction

Conclusions

References

Tables

Figures



Back

Close

Full Screen / Esc

Printer-friendly Version

Interactive Discussion



- Gettelman, A., Salby, M. L., and Sassi, F.: Distribution and influence of convection in the tropical tropopause region, *J. Geophys. Res.*, 107, 4080, doi:10.1029/2001JD001048, 2002.
- Gettelman, A., Hoor, P., Pan, L. L., Randel, W. J., Hegglin, M. I., and Birner, T.: The extratropical upper troposphere and lower stratosphere, *Rev. Geophys.*, 49, RG3003, doi:10.1029/2011RG000355, 2011.
- Glatthor, N., von Clarmann, T., Fischer, H., Funke, B., Grabowski, U., Höpfner, M., Kellmann, S., Kiefer, M., Linden, A., Milz, M., Steck, T., and Stiller, G. P.: Global peroxyacetyl nitrate (PAN) retrieval in the upper troposphere from limb emission spectra of the Michelson Interferometer for Passive Atmospheric Sounding (MIPAS), *Atmos. Chem. Phys.*, 7, 2775–2787, doi:10.5194/acp-7-2775-2007, 2007.
- Grewe, V., Brunner, D., Dameris, M., Grenfell, J. L., Hein, R., Shindell, D., and Staehelin, J.: Origin and variability of upper tropospheric nitrogen oxides and ozone at northern mid-latitudes, *Atmos. Environ.*, 35, 3421–3433, 2001.
- Harriss, R. C., Wofsy, S. C., Garstang, M., Browell, E. V., Molion, L. C. B., McNeal, R. J., Hoell Jr., J. M., Bendura, R. J., Beck, S. M., Navarro, R. L., Riley, J. T., and Snell, R. L.: The Amazon boundary layer experiment (ABLE 2A) dry season 1985, *J. Geophys. Res.*, 93, 1351–1360, 1988.
- Harriss, R. C., Wofsy, S. C., Bartlett, D. S., Shipham, M. C., Jacob, D. J., Hoell Jr., J. M., Bendura, R. J., Drewry, J. W., McNeal, R. J., Navarro, R. L., Gidge, R. N., and Rabine, V. E.: The Arctic Boundary Layer Expedition (ABLE 3A): July–August 1988, *J. Geophys. Res.*, 97, 16383–16394, 1992.
- Harriss, R. C., Wofsy, S. C., Hoell Jr., J. M., Bendura, R. J., Drewry, J. W., McNeal, R. J., Pierce, D., Rabine, V., and Snell, R. L.: The Arctic Boundary Layer Expedition (ABLE-3B): July–August 1990, *J. Geophys. Res.*, 99, 1635–1643, 1994.
- Hassim, M. E. E., Lane, T. P., and May, P. T.: Ground-based observations of overshooting convection during the tropical warm pool-international cloud experiment, *J. Geophys. Res.-Atmos.*, 119, 880–905, doi:10.1002/2013JD020673, 2014.
- Hoell Jr., J. M., Albritton, D. L., Gregory, G. L., McNeal, R. J., Beck, S. M., Bendura, R. J., and Drewry, J. W.: Operational overview of NASA GTE/CITE 2 airborne instrumentinter-comparisons: nitrogen dioxide, nitric acid, and peroxyacetyl nitrate, *J. Geophys. Res.*, 95, 10047–10054, 1990.
- Horowitz, L. W., Walters, S., Mauzerall, D. L., Emmons, L. K., Rasch, P. J., Granier, C., Tie, X., Lamarque, J., Schultz, M. G., Tyndall, G. S., Orlando, J. J., and Brasseur, G. P.: A global

Transport pathways of peroxyacetyl nitrate

S. Fadnavis et al.

Title Page

Abstract

Introduction

Conclusions

References

Tables

Figures



Back

Close

Full Screen / Esc

Printer-friendly Version

Interactive Discussion



simulation of tropospheric ozone and related tracers, description and evaluation of MOZART, version 2, *J. Geophys. Res.*, 108, 4784, doi:10.1029/2002JD002853, 2003.

Hudman, R. C., Jacob, D. J., Cooper, O. R., Evans, M. J., Heald, C. L., Park, R. J., Fehsenfeld, F., Flocke, F., Holloway, J., Hübler, G., Kita, K., Koike, M., Kondo, Y., Neuman, A., Nowak, J., Oltmans, S., Parrish, D., Roberts, J. M., and Ryerson, T.: Ozone production in transpacific Asian pollution plumes and implications for ozone air quality in California, *J. Geophys. Res.*, 109, D23S10, doi:10.1029/2004jd004974, 2004.

Hudman, R. C., Jacob, D. J., Turquety, S., Leibensperger, E. M., Murray, L. T., Wu, S., Gilliland, A. B., Avery, M., Bertram, T. H., Brune, W., Cohen, R. C., Dibb, J. E., Flocke, F. M., Fried, A., Holloway, J., Neuman, J. A., Orville, R., Perring, A., Ren, X., Ryerson, T. B., Sachse, G. W., Singh, H. B., Swanson, A., and Wooldridge, P. J.: Surface and lightning sources of nitrogen oxides over the United States: magnitudes, chemical evolution, and outflow, *J. Geophys. Res.*, 112, D12S05, doi:10.1029/2006JD007912, 2007.

Keim, C., Liu, G. Y., Blom, C. E., Fischer, H., Gulde, T., Höpfner, M., Piesch, C., Ravegnani, F., Roiger, A., Schlager, H., and Sitnikov, N.: Vertical profile of peroxyacetyl nitrate (PAN) from MIPAS-STR measurements over Brazil in February 2005 and its contribution to tropical UT NO_y partitioning, *Atmos. Chem. Phys.*, 8, 4891–4902, doi:10.5194/acp-8-4891-2008, 2008.

Khaykin, S., Pommereau, J.-P., Korshunov, L., Yushkov, V., Nielsen, J., Larsen, N., Christensen, T., Garnier, A., Lukyanov, A., and Williams, E.: Hydration of the lower stratosphere by ice crystal geysers over land convective systems, *Atmos. Chem. Phys.*, 9, 2275–2287, doi:10.5194/acp-9-2275-2009, 2009.

Kulkarni, J. R., Maheshkumar, R. S., Morwal, S. B., Padma kumari, B., Konwar, M., Deshpande, C. G., Joshi, R. R., Bhalwankar, R. V., Pandithurai, G., Safai, P. D., Narkhedkar, S. G., Dani, K. K., Nath, A., Nair, Sathy, Sapre, V. V., Puranik, P. V., Kandalgaonkar, S. S., Mujumdar, V. R., Khaladkar, R. M., Vijaykumar, R., Prabha, T. V., Goswami, B. N.: The Cloud Aerosol Interaction and Precipitation Enhancement Experiment (CAIPEEX): overview and preliminary results, *Curr. Sci. India*, 102, 413–425, 2012.

Labrador, L. J., von Kuhlmann, R., and Lawrence, M. G.: The effects of lightning-produced NO_x and its vertical distribution on atmospheric chemistry: sensitivity simulations with MATCH-MPIC, *Atmos. Chem. Phys.*, 5, 1815–1834, doi:10.5194/acp-5-1815-2005, 2005.

Lamsal, L. N., Martin, R. V., Padmanabhan, A., van Donkelaar, A., Zhang, Q., Sioris, C. E., Chance, K., Kurosu, T. P., and Newchurch, M. J.: Application of satellite observations for

**Transport pathways
of peroxyacetyl
nitrate**

S. Fadnavis et al.

Title Page

Abstract

Introduction

Conclusions

References

Tables

Figures



Back

Close

Full Screen / Esc

Printer-friendly Version

Interactive Discussion



timely updates to global anthropogenic NO_x emission inventories, *Geophys. Res. Lett.*, **38**, L05810, doi:10.1029/2010GL046476, 2011.

Li, Q., Jiang, J. H., Wu, D. L., Read, W. G., Livesey, N. J., Waters, J. W., Zhang, Y., Wang, B., Filipiak, M. J., Davis, C. P., Turquety, S., Wu, S., Park, R. J., Yantosca, R. M., and Jacob, D. J.: Convective outflow of South Asian pollution: a global CTM simulation compared with EOS MLS observations, *Geophys. Res. Lett.*, **32**, L14826, doi:10.1029/2005GL022762, 2005.

Liang, Q., Rodriguez, J. M., Douglass, A. R., Crawford, J. H., Olson, J. R., Apel, E., Bian, H., Blake, D. R., Brune, W., Chin, M., Colarco, P. R., da Silva, A., Diskin, G. S., Duncan, B. N., Huey, L. G., Knapp, D. J., Montzka, D. D., Nielsen, J. E., Pawson, S., Riemer, D. D., Weinheimer, A. J., and Wisthaler, A.: Reactive nitrogen, ozone and ozone production in the Arctic troposphere and the impact of stratosphere-troposphere exchange, *Atmos. Chem. Phys.*, **11**, 13181–13199, doi:10.5194/acp-11-13181-2011, 2011.

Liu, C. and Zipser, E. J.: Global distribution of convection penetrating the tropical tropopause, *J. Geophys. Res.*, **110**, D23104, doi:10.1029/2005JD006063, 2005.

Martin, R. V., Sauvage, B., Folkins, I., Sioris, C. E., Boone, C., Bernath, P., and Ziemke, J.: Space-based constraints on the production of nitric oxide by lightning, *J. Geophys. Res.*, **112**, D09309, doi:10.1029/2006JD007831, 2007.

Miyazaki, K., Eskes, H. J., and Sudo, K.: Global NO_x emission estimates derived from an assimilation of OMI tropospheric NO₂ columns, *Atmos. Chem. Phys.*, **12**, 2263–2288, doi:10.5194/acp-12-2263-2012, 2012.

Murray, L. T., Jacob, D. J., Logan, J. A., Hudman, R. C., and Koshak, W. J.: Optimized regional and interannual variability of lightning in a global chemical transport model constrained by LIS/OTD satellite data, *J. Geophys. Res.*, **117**, D20307, doi:10.1029/2012JD017934, 2012.

O'Sullivan, D. W., Heikes, B. G., Lee, M., Chang, W., Gregory, G. L., Blake, D. R., and Sachs, G. W.: Distribution of hydrogen peroxide and methylhydroperoxide over the Pacific and South Atlantic Oceans, *J. Geophys. Res.*, **104**, 5635–5646, 1999.

Pan, L. L., Kunz, A., Homeyer, C. R., Munchak, L. A., Kinnison, D. E., and Tilmes, S.: Commentary on using equivalent latitude in the upper troposphere and lower stratosphere, *Atmos. Chem. Phys.*, **12**, 9187–9199, doi:10.5194/acp-12-9187-2012, 2012.

Park, M., Randel, W. J., Kinnison, D. E., Garcia, R. R., and Choi, W.: Seasonal variation of methane, water vapour, and nitrogen oxides near the tropopause: satellite observations and model simulations, *J. Geophys. Res.*, **109**, D03302, doi:10.1029/2003JD003706, 2004.

Transport pathways of peroxyacetyl nitrate

S. Fadnavis et al.

Title Page

Abstract

Introduction

Conclusions

References

Tables

Figures



Back

Close

Full Screen / Esc

Printer-friendly Version

Interactive Discussion



Park, M., Randel, W. J., Gettleman, A., Massie, S. T., and Jiang, J. H.: Transport above the Asian summer monsoon anticyclone inferred from aura microwave limb sounder tracers, *J. Geophys. Res.*, 112, D16309, doi:10.1029/2006JD008294, 2007.

Park, M., Randel, W. J., Emmons, L. K., and Livesey, N. J.: Transport pathways of carbon monoxide in the Asian summer monsoon diagnosed from Model of Ozone and Related Tracers (MOZART), *J. Geophys. Res.*, 114, D08303, doi:10.1029/2008JD010621, 2009.

Penki, R. K. and Kamra, A. K.: Lightning distribution with respect to the monsoon trough position during the Indian summer monsoon season, *J. Geophys. Res.*, 118, 4780–4787, doi:10.1002/jgrd.50382, 2013.

Pozzoli, L., Bey, I., Rast, J. S., Schultz, M. G., Stier, P., and Feichter, J.: Trace gas and aerosol interactions in the fully coupled model of aerosol-chemistry-climate ECHAM5-HAMMOZ: 1. Model description and insights from the spring 2001 TRACE-P experiment, *J. Geophys. Res.*, 113, D07308, doi:10.1029/2007JD009007, 2008a.

Pozzoli, L., Bey, I., Rast, J. S., Schultz, M. G., Stier, P., and Feichter, J.: Trace gas and aerosol interactions in the fully coupled model of aerosol-chemistry-climate ECHAM5-HAMMOZ: 2. Impact of heterogeneous chemistry on the global aerosol distributions, *J. Geophys. Res.*, 113, D07309, doi:10.1029/2007JD009008, 2008b.

Pozzoli, L., Janssens-Maenhout, G., Diehl, T., Bey, I., Schultz, M. G., Feichter, J., Vignati, E., and Dentener, F.: Re-analysis of tropospheric sulfate aerosol and ozone for the period 1980–2005 using the aerosol-chemistry-climate model ECHAM5-HAMMOZ, *Atmos. Chem. Phys.*, 11, 9563–9594, doi:10.5194/acp-11-9563-2011, 2011.

Prabha, T. V., Khain, A., Maheshkumar, R. S., Pandithurai, G., Kulkarni, J. R., and Goswami, B. N.: Microphysics of premonsoon and monsoon clouds as seen from in situ measurements during the Cloud Aerosol Interaction and Precipitation Enhancement Experiment (CAIPEEX), *J. Atmos. Sci.*, 68, 1882–1901, doi:10.1175/2011JAS3707.1, 2011.

Price, C. and Asfur, M.: Inferred long term trends in lightning activity over Africa, *Earth Planets Space*, 58, 1197–1201, 2006.

Ranalkar, M. R. and Chaudhari, H. S.: Seasonal variation of lightning activity over the Indian subcontinent, *Meteorol. Atmos. Phys.*, 104, 125–134, 2009.

Randel, W. J. and Park, M.: Deep convective influence on the Asian summer monsoon anticyclone and associated tracer variability observed with Atmospheric Infrared Sounder (AIRS), *J. Geophys. Res.*, 111, D12314, doi:10.1029/2005JD006490, 2006.

Transport pathways of peroxyacetyl nitrate

S. Fadnavis et al.

Title Page

Abstract

Introduction

Conclusions

References

Tables

Figures



Back

Close

Full Screen / Esc

Printer-friendly Version

Interactive Discussion



Randel, W. J., Park, M., Emmons, L., Kinnison, D., Bernath, P., Walker, K. A., Boone, C., and Pumphrey, H.: Asian monsoon transport of pollution to the stratosphere, *Science*, 328, 611–613, 2010.

Randel, W. J., Moyer, E., Park, M., Jensen, E., Bernath, P., Walker, K., and Boone, C.: Global variations of HDO and HDO/H₂O ratios in the upper troposphere and lower stratosphere derived from ACE-FTS satellite measurements, *J. Geophys. Res.*, 117, D06303, doi:10.1029/2011JD016632, 2012.

Real, E., Orlandi, E., Law, K. S., Fierli, F., Josset, D., Cairo, F., Schlager, H., Borrmann, S., Kunkel, D., Volk, C. M., McQuaid, J. B., Stewart, D. J., Lee, J., Lewis, A. C., Hopkins, J. R., Ravegnani, F., Ulanovski, A., and Liousse, C.: Cross-hemispheric transport of central African biomass burning pollutants: implications for downwind ozone production, *Atmos. Chem. Phys.*, 10, 3027–3046, doi:10.5194/acp-10-3027-2010, 2010.

Ridley, B. A., Madronich, S., Chatfield, R. B., Walega, J. G., Shetter, R. E., Carroll, M. A., and Montzka, D. D: Measurements and model simulations of the photostationary state during the Mauna Loa Observatory Photochemistry Experiment: implications for radical concentrations and ozone production and loss rates, *J. Geophys. Res.*, 97, 10375–10388, doi:10.1029/91JD02287, 1992.

Ridley, B. A., Walega, J. G., Dye, J. E., and Grahek, F. E.: Distributions of NO, NO_x, NO_y, and O₃ to 12 km altitude during the summer monsoon season over New Mexico, *J. Geophys. Res.*, 99, 25519–25534, 1994.

Roeckner, E., Bauml, G., Bonaventura, L., Brokopf, R., Esch, M., Giorgetta, M., Hagemann, S., Kirchner, I., Kornbluh, L., Manzini, E., Rhodin, A., Schlese, U., Schulzweida, U., and Tompkins, A.: The atmospheric general circulation model ECHAM5: Part 1, Tech. Rep. 349, Max Planck Institute for Meteorology, Hamburg, 2003.

Sander, S. P., Friedl, R. R., Ravishankara, A. R., Golden, D. M., Kolb, C. E., Kurylo, M. J., Huie, R. E., Orkin, V. L., Molina, M. J., Moortgat, G. K., and Finlayson-Pitts, B. J.: Chemical kinetics and photochemical data for use in atmospheric studies, evaluation number 14, JPL Publ. 02–25, Jet Propul. Lab., Calif. Inst. of Technol., Pasadena, available at: http://jpldataeval.jpl.nasa.gov/pdf/JPL_02-25_rev02.pdf (last access: 28 May 2015), 2003.

Schmitz, J. T. and Mullen, S. L.: Water vapor transport associated with the summertime North American Monsoon as depicted by ECMWF analyses, *J. Climate*, 9, 1621–1634, 1996.

Schultz, M., Backman, L., Balkanski, Y., Bjoerndalsaeter, S., Brand, R., Burrows, J., Dalsoeren, S., de Vasconcelos, M., Grodtmann, B., Hauglustaine, D., Heil, A., Hoelzemann, J.,

**Transport pathways
of peroxyacetyl
nitrate**

S. Fadnavis et al.

Title Page

Abstract

Introduction

Conclusions

References

Tables

Figures



Back

Close

Full Screen / Esc

Printer-friendly Version

Interactive Discussion



Isaksen, I., Kaurola, J., Knorr, W., Ladstaetter-Weienmayer, A., Mota, B., Oom, D., Pa-
cyna, J., Panasiuk, D., Pereira, J., Pulles, T., Pyle, J., Rast, S., Richter, A., Savage, N.,
Schnadt, C., Schulz, M., Spessa, A., Staehelin, J., Sundet, J., Szopa, S., Thonicke, K., van
het Bolscher, M., van Noije, T., van Velthoven, P., Vik, A., and Wittrock, F.: REanalysis of the
5 TROpospheric chemical composition over the past 40 years (RETRO). A long-term global
modeling study of tropospheric chemistry. Final Report, Tech. rep., Max Planck Institute for
Meteorology, Hamburg, Germany, 2007.

Schultz, M. G., Heil, A., Hoelzemann, J. J., Spessa, A., Thonicke, K., Goldammer, J. G.,
Held, A. C., Pereira, J. M. C., and van het Bolscher, M.: Global wildland fire emissions from
10 1960 to 2000, *Global Biogeochem. Cy.*, 22, GB2002, doi:10.1029/2007GB003031, 2008.

Schultz, M. G., Pulles, T., Brand, R., Van het Bolscher, M., and Dalsøren, S. T.: A global data
set of anthropogenic CO, NO_x, and NMVOC emissions for 1960–2000, available at: <http://eccad.sedoo.fr/> (last access: 28 May 2015), in preparation, 2015.

Schumann, U. and Huntrieser, H.: The global lightning-induced nitrogen oxides source, *Atmos.*
15 *Chem. Phys.*, 7, 3823–3907, doi:10.5194/acp-7-3823-2007, 2007.

Shepon, A., Gildor, H., Labrador, L. J., Butler, T., Ganzeveld, L. N., and Lawrence, M. G.:
Global reactive nitrogen deposition from lightning NO_x, *J. Geophys. Res.*, 112, D06304,
doi:10.1029/2006JD007458, 2007.

Singh, H. B.: Reactive nitrogen in the troposphere, *Environ. Sci. Technol.*, 21, 320–327, 1987.

20 Singh, H. B., Salas, L. J., and Viezee, W.: Global distribution of peroxyacetyl nitrate, *Nature*,
321, 588–591, 1986.

Singh, H. B., Viezee, W., Chen, Y., Thakur, A. N., Kondo, Y., and Talbot, R. W., Gregory, G. L.,
Sachse, G. W., Blake, D. R., Bradshaw, J. D., Wang, Y., and Jacob, D. J.: Latitudinal distri-
bution of reactive nitrogen in the free troposphere over the Pacific Ocean in late winter/early
25 spring, *J. Geophys. Res.*, 103, 28237–28246, doi:10.1029/98JD01891, 1998.

Singh, H. B., Brune, W. H., Crawford, J. H., Jacob, D. J., and Russell, P. B.: Overview of the sum-
mer 2004 Intercontinental Chemical Transport Experiment – North America (INTEX-A), *J.*
Geophys. Res., 111, D24S01, doi:10.1029/2006JD007905, 2006.

30 Stier, P., Feichter, J., Kinne, S., Kloster, S., Vignati, E., Wilson, J., Ganzeveld, L., Tegen, I.,
Werner, M., Balkanski, Y., Schulz, M., Boucher, O., Minikin, A., and Petzold, A.: The aerosol-
climate model ECHAM5-HAM, *Atmos. Chem. Phys.*, 5, 1125–1156, doi:10.5194/acp-5-1125-
2005, 2005.

**Transport pathways
of peroxyacetyl
nitrate**

S. Fadnavis et al.

Title Page

Abstract

Introduction

Conclusions

References

Tables

Figures



Back

Close

Full Screen / Esc

Printer-friendly Version

Interactive Discussion



Talbot, R. W., Dibb, J. E., Scheuer, E. M., Bradshaw, J. D., Sandholm, S. T., Singh, H. B., Blake, D. R., Blake, N. J., Atlas, E., and Flocke, F.: Tropospheric reactive odd nitrogen over the South Pacific in austral springtime, *J. Geophys. Res.*, 105, 6681–6694, doi:10.1029/1999JD901114, 2000.

5 Talukdar, R. K., Burkholder, J. B., Schmoltner, A., Roberts, J. M., Wilson, R. R., and Ravishankara, A. R.: Investigation of loss processes for peroxyacetyl nitrate in the atmosphere: UV photolysis and reaction with OH, *J. Geophys. Res.*, 100, 14163–14173, 1995.

Tang, J. H., Chan, L. Y., Chang, C. C., Liu, S., and Li, Y. S.: Characteristics and sources of non-methane hydrocarbons in background atmospheres of eastern, southwestern, and southern
10 China, *J. Geophys. Res.*, 114, D03304, doi:10.1029/2008JD010333, 2009.

Tereszchuk, K. A., Moore, D. P., Harrison, J. J., Boone, C. D., Park, M., Remedios, J. J., Randel, W. J., and Bernath, P. F.: Observations of peroxyacetyl nitrate (PAN) in the upper troposphere by the Atmospheric Chemistry Experiment-Fourier Transform Spectrometer (ACE-FTS), *Atmos. Chem. Phys.*, 13, 5601–5613, doi:10.5194/acp-13-5601-2013, 2013.

15 Tie, X. X., Zhang, R., Brasseur, G., Emmons, L., and Lei, W.: Effects of lightning on reactive nitrogen and nitrogen reservoir species in the troposphere, *J. Geophys. Res.-Atmos.*, 106, 3167–3178, doi:10.1029/2000JD900565, 2001.

Vaughan, G. and Timmis, C.: Transport of near-tropopause air into the lower midlatitude stratosphere, *Q. J. Roy. Meteorol. Soc.*, 124, 1559–1578, 1998.

20 von Clarmann, T., Höpfner, M., Kellmann, S., Linden, A., Chauhan, S., Funke, B., Grabowski, U., Glatthor, N., Kiefer, M., Schieferdecker, T., Stiller, G. P., and Versick, S.: Retrieval of temperature, H₂O, O₃, HNO₃, CH₄, N₂O, ClONO₂ and ClO from MIPAS reduced resolution nominal mode limb emission measurements, *Atmos. Meas. Tech.*, 2, 159–175, doi:10.5194/amt-2-159-2009, 2009.

25 Wiegele, A., Glatthor, N., Höpfner, M., Grabowski, U., Kellmann, S., Linden, A., Stiller, G., and von Clarmann, T.: Global distributions of C₂H₆, C₂H₂, HCN, and PAN retrieved from MIPAS reduced spectral resolution measurements, *Atmos. Meas. Tech.*, 5, 723–734, doi:10.5194/amt-5-723-2012, 2012.

Xiong, X., Houweling, S., Wei, J., Maddy, E., Sun, F., and Barnet, C.: Methane plume over south
30 Asia during the monsoon season: satellite observation and model simulation, *Atmos. Chem. Phys.*, 9, 783–794, doi:10.5194/acp-9-783-2009, 2009.

Zhang, L., Jacob, D. J., Boersma, K. F., Jaffe, D. A., Olson, J. R., Bowman, K. W., Worden, J. R., Thompson, A. M., Avery, M. A., Cohen, R. C., Dibb, J. E., Flock, F. M., Fuelberg, H. E.,

Table 1. Global aircraft measurements used for model evaluation.

Experiment	Date Frame	Species	Location
<u>POLINAT-2</u> (Falcon), Ziereis et al. (2000)	19 Sep–Oct 25, 1997	O ₃ , NO _x	Canary-Islands: LAT = 25, 35° N, LON = 160, 170° W, E-Atlantic: LAT = 35, 45° N, LON = 150, 160° W, Europe: LAT = 45, 55° N, LON = 5, 15° E, Ireland: LAT = 50, 60° N, LON = 165, 175° W
<u>PEM-Tropics-A</u> (DC8), Talbot et al. (2000)	24 Aug–15 Oct 1996	O ₃ , NO _x , HNO ₃ , PAN	Christmas-Island: LAN = 0, 10° N, LON = 20, 40° W, Easter-Island: LAT = -40° N, 20° S, LON = 60, 80° W, Fiji: LAT = 0°, 10° S, LON = 170° E, 10° W, Hawaii: LAT = 10, 30° N, LON = 10, 30° W, Tahiti: LAT = 20° S, 0°, LON = 20, 50° W
<u>PEM-Tropics-A</u> (P3), O'Sullivan et al. (1999)	15 Aug–26 Sep 1996	O ₃ , HNO ₃	Christmas-Island: LAT = 0°, 10° N, LON = 20, 40° W, Easter-Island: LAT = 40, 20° S, LON = 60, 80° W, Hawaii: LAT = 10, 30° N, LON = 10, 30° W, Tahiti: LAT = 20° S, 0°, LON = 20, 50° W
<u>ABLE-3B</u> (Electra), Harriss et al. (1994)	6 Jul–15 Aug 1990	O ₃ , NO _x , HNO ₃ , PAN	Labrador: LAT = 50, 55° N, LON = 120, 135° W, Ontario: LAT = 45, 60° N, LON = 90, 100° W, US-E-Coast: LAT = 35, 45° N, LON = 100, 110° W, Natal: LAT = 15° S, 5° N, LON = 145, 155° W, Wallops: LAT = 30, 40° N, LON = 100, 110° W, New-Mexico: LAT = 30, 35° N, LON = 70, 75° W
CITE-3 (Electra), Hoell et al. (1993)	22 Aug–29 Sep 1989	O ₃ , NO _x	
ELCHEM (Sabreliner), Ridley et al. (1999)	27 Jul–22 Aug 1989	O ₃ , NO _x	
<u>ABLE-3A</u> (Electra), Harriss et al. (1992)	7 Jul–17 Aug 1988	O ₃ , NO _x , PAN	Alaska: LAT = 55, 75° N, LON = 10, 25° W
<u>ABLE-2A</u> (Electra), Harris et al. (1988)	12 Jul–13 Aug 1985	O ₃	E-Brazil: LAT = 10° S, 0°, LON = 120, 135° W, W-Brazil: LAT = 5° S, 0°, LON = 110, 120° W
STRAT0Z-3 (Caravelle 116), Drummond et al. (1988)	4–26 Jun 1984	O ₃	Brazil: LAT = 20° S, 0°, LON = 135, 155° W, Canary-Islands: LAT = 20, 35° N, LON = 160, 155° W, E-Tropical-N-Atlantic: LAT = 0°, 20° N, LON = 150, 165° W, England: LAT = 45, 60° N, LON = 10° E, 5° W, Goose-Bay: LAT = 45, 60° N, LON = 110, 125° W, Greenland: LAT = 60, 70° N, LON = 110, 150° W, Iceland: LAT = 60, 70° N, LON = 150, 155° W, NW-South-America: LAT = -5, 10° N, LON = 95, 115° W, Puerto-Rico: LAT = 10, 25° N, LON = 110, 120° W, S-South-America: LAT = 65, 45° S, LON = 95, 120° W, SE-South-America: LAT = 45, 20° S, LON = 115, 140° W, SW-South-America: LAT = -45, 25° S, LON = 105, 112° W, Spain: LAT = 35, 45° N, LON = 15° W, 0°, W-Africa: LAT = 0°, 15° N, LON = 15° W, 0°, W-South-America: LAT = 25, 5° S, LON = 95, 110° W, Western-N-Atlantic: LAT = 25, 45° N, LON = 110, 120° W
<u>CITE-2</u> (Electra), Hoell et al. (1990)	11 Aug–5 Sep 1986	O ₃ , NO _x , HNO ₃ , PAN	Calif: LAT = 35, 45° N, LON = 55, 70° W, Pacific: LAT = 30, 45° N, LON = 45, 55° W
INTEX-A, Singh et al. (2006) CAIPEEX, Prabha et al. (2011)	Jul–Aug 2004 Sep–Oct 2010	O ₃ , PAN, NO _x O ₃ , NO _x	Eastern North America: LAT = 29, 51° N, LON: 44–120° W LAT = 12, 22° N, LON = 74, 78° E

Title Page

Abstract

Introduction

Conclusions

References

Tables

Figures



Back

Close

Full Screen / Esc

Printer-friendly Version

Interactive Discussion



Transport pathways of peroxyacetyl nitrate

S. Fadnavis et al.

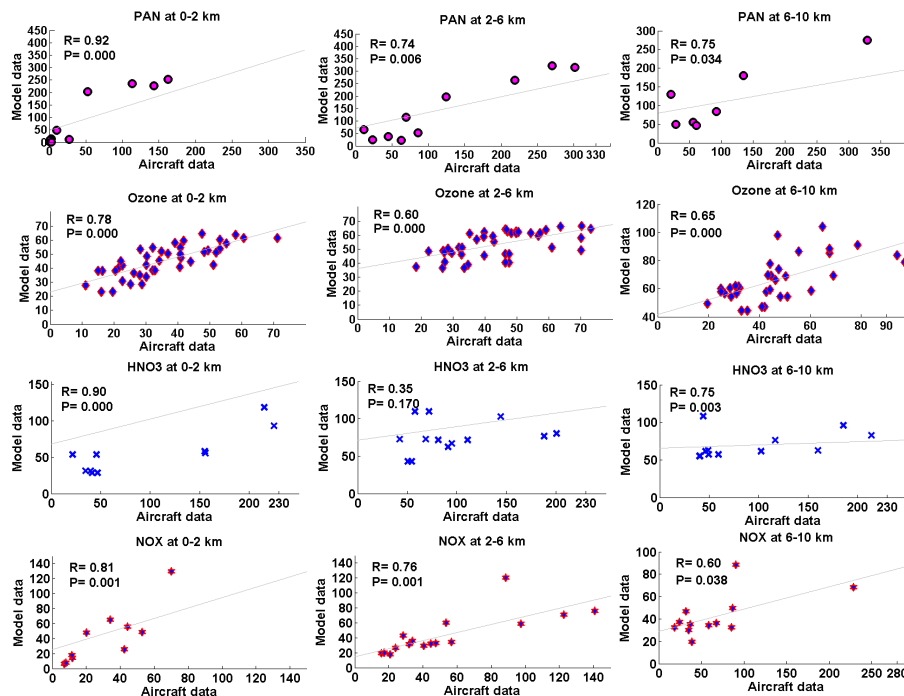


Figure 2. Scatter plot between model simulation (averaged for 1995–2004) and aircraft observations of PAN (ppt), ozone (ppb), HNO₃ (ppt), NO_x (ppt) (averaged for the monsoon season (June–September)). The model simulations and aircraft observations are averaged for altitude ranges over the coherent regions. The Pearson's correlation coefficient (R) and corresponding p value is given in each subplot.

Transport pathways
of peroxyacetyl
nitrate

S. Fadnavis et al.

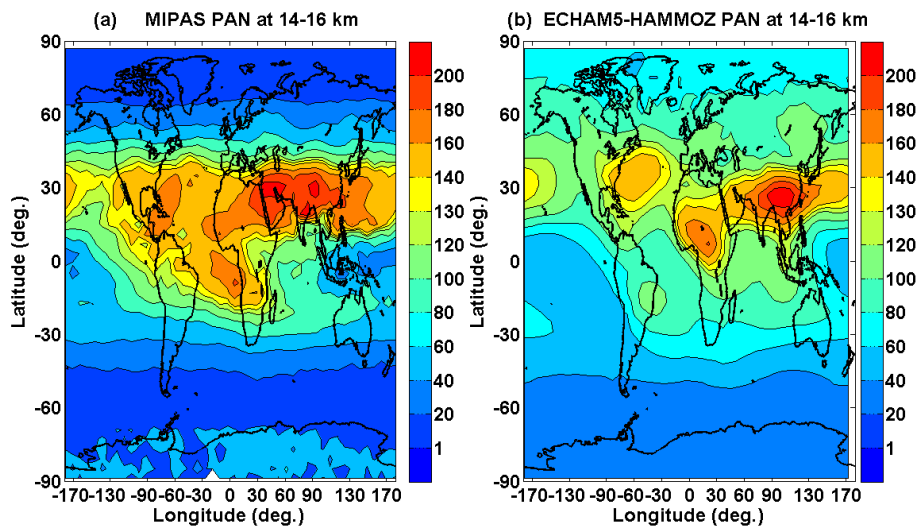


Figure 3. Distribution of seasonal mean PAN concentration (ppt) averaged for 14–16 km **(a)** observed by MIPAS-E (climatology for the period 2002–2011) **(b)** ECHAM5-HAMMOZ CTRL simulations.

[Title Page](#)[Abstract](#)[Introduction](#)[Conclusions](#)[References](#)[Tables](#)[Figures](#)[◀](#)[▶](#)[◀](#)[▶](#)[Back](#)[Close](#)[Full Screen / Esc](#)[Printer-friendly Version](#)[Interactive Discussion](#)

Transport pathways
of peroxyacetyl
nitrate

S. Fadnavis et al.

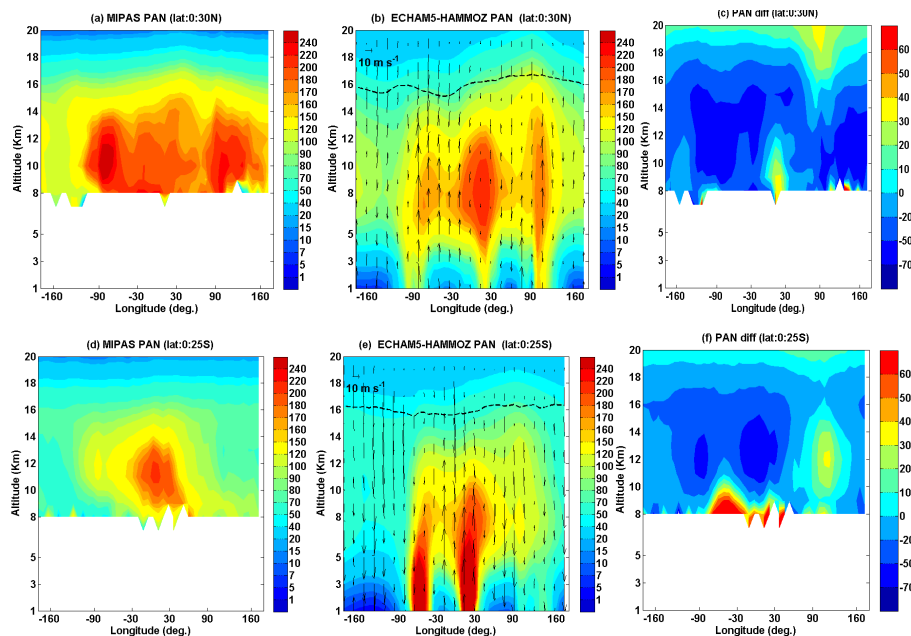


Figure 4. Longitude–altitude cross section of PAN (ppt) averaged for monsoon season and 10–30° N; **(a)** MIPAS-E climatology **(b)** ECHAM5-HAMMOZ CTRL simulations. **(c)** Difference in PAN (ppt) (MIPAS-ECHAM5-HAMMOZ). PAN (ppt) averaged for monsoon season and 0–25° S **(d)** MIPAS-E climatology **(e)** ECHAM5-HAMMOZ CTRL simulations **(f)** difference in PAN (ppt) (MIPAS-ECHAM5-HAMMOZ). ECHAM5-HAMMOZ simulations are smoothed with averaging kernel of MIPAS-E. Wind vectors are indicated by black arrows in figures **(b, e)**. The vertical velocity field has been scaled by 300. The black line in **(b, e)** indicates the tropopause.

Title Page

Abstract

Introduction

Conclusions

References

Tables

Figures



Back

Close

Full Screen / Esc

Printer-friendly Version

Interactive Discussion



Transport pathways of peroxyacetyl nitrate

S. Fadnavis et al.

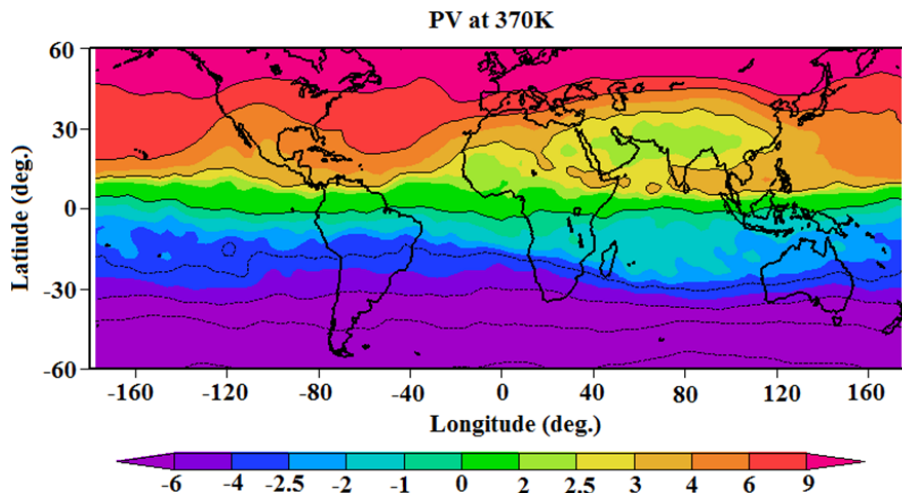


Figure 5. Map of potential vorticity in PV units ($1 \text{ PVU} = 10^{-6} \text{ Km}^2 \text{ kg}^{-1} \text{ s}^{-1}$) on the 370 K level for the monsoon season obtained from ECHAM5-HAMMOZ CTRL simulations.

[Title Page](#)[Abstract](#)[Introduction](#)[Conclusions](#)[References](#)[Tables](#)[Figures](#)[◀](#)[▶](#)[◀](#)[▶](#)[Back](#)[Close](#)[Full Screen / Esc](#)[Printer-friendly Version](#)[Interactive Discussion](#)

Transport pathways of peroxyacetyl nitrate

S. Fadnavis et al.

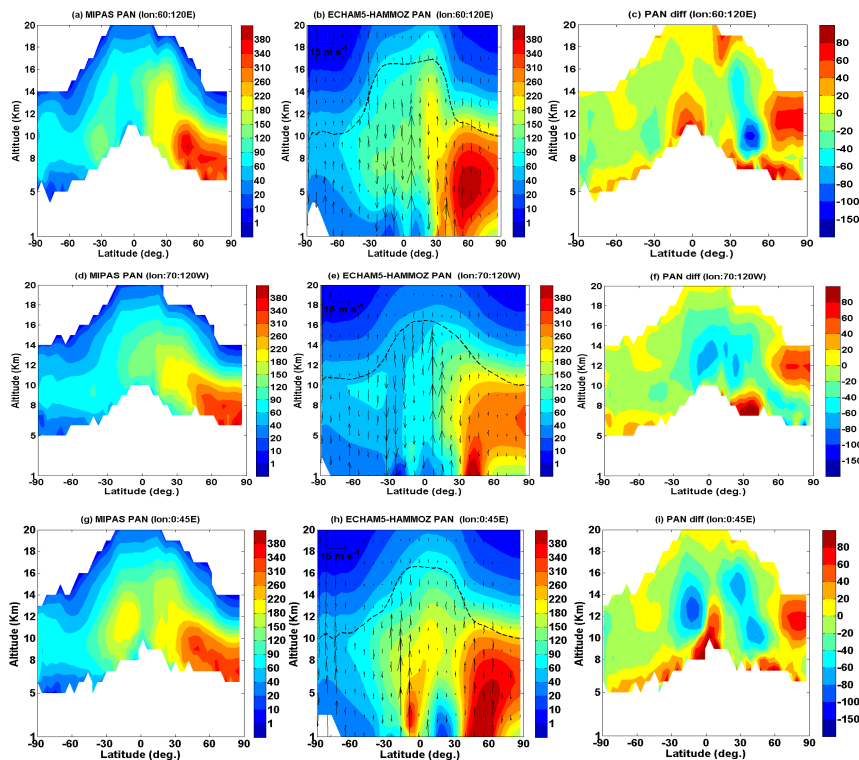


Figure 6. Latitude–altitude cross section of PAN (ppt) **(a)** MIPAS-E climatology, averaged for monsoon season and 60–120° E, **(b)** PAN from ECHAM5-HAMMOZ CTRL simulations, averaged for monsoon season and 60–120° E, **(c)** difference in PAN (ppt) (MIPAS-ECHAM5-HAMMOZ), **(d)** same as **(a)** but averaged over 70–120° W, **(e)** same as **(b)** but averaged over 70–120° W, **(f)** difference in PAN (ppt) (MIPAS-ECHAM5-HAMMOZ), **(g)** same as **(a)** but averaged over 0–45° E, **(h)** same as **(b)** but averaged for 0–45° E, **(i)** difference in PAN (ppt) (MIPAS-ECHAM5-HAMMOZ). Wind vectors are indicated by black arrows in figures **(b)**, **(e)**, **(f)**. The vertical velocity field has been scaled by 300.

Title Page

Abstract

Introduction

Conclusions

References

Tables

Figures



Back

Close

Full Screen / Esc

Printer-friendly Version

Interactive Discussion



Transport pathways of peroxyacetyl nitrate

S. Fadnavis et al.

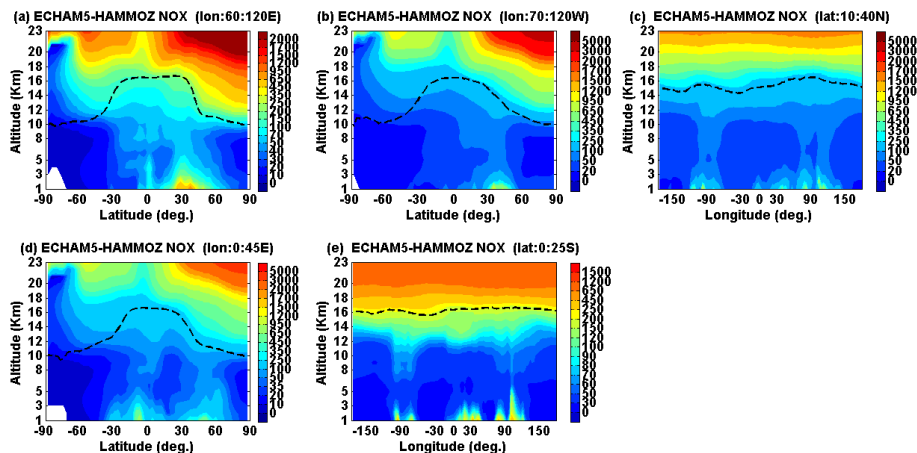


Figure 7. Panel (a) Latitude–altitude cross section of seasonal mean ECHAM5-HAMMOZ NO_x (ppt) averaged for (a) 60–120° E (b) 70–120° W (c) longitude–altitude cross section averaged over 10–40° N (d) latitude–altitude cross section averaged over 0–45° E and (e) longitude–altitude cross section averaged over 0–25° S.

Title Page

Abstract

Introduction

Conclusions

References

Tables

Figures

◀

▶

◀

▶

Back

Close

Full Screen / Esc

Printer-friendly Version

Interactive Discussion



Transport pathways
of peroxyacetyl
nitrate

S. Fadnavis et al.

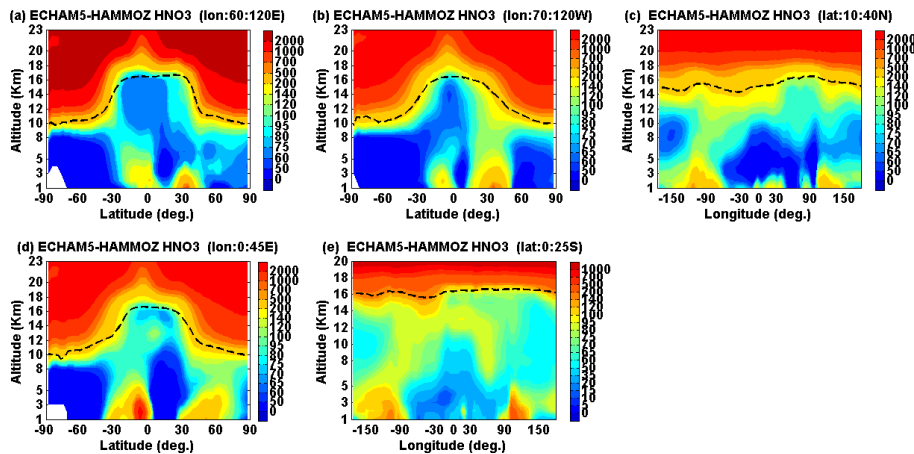


Figure 8. Same as Fig. 6 but for HNO₃ (ppt).

[Title Page](#)[Abstract](#)[Introduction](#)[Conclusions](#)[References](#)[Tables](#)[Figures](#)[Back](#)[Close](#)[Full Screen / Esc](#)[Printer-friendly Version](#)[Interactive Discussion](#)

Transport pathways of peroxyacetyl nitrate

S. Fadnavis et al.

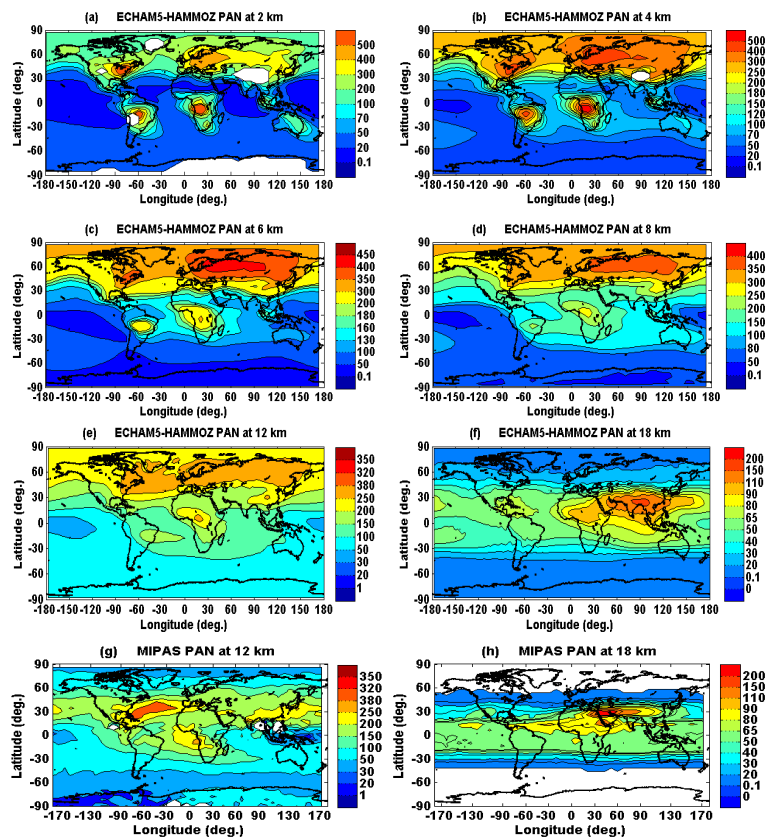


Figure 9. Latitude–longitude cross section of PAN (ppt) averaged for monsoon season (a) ECHAM5-HAMMOZ simulations at 2 km (b) 4 km (c) 6 km (d) 8 km (e) 12 km (f) 18 km. MIPAS-E climatology at (g) 12 km (h) 18 km.

Title Page

Abstract

Introduction

Conclusions

References

Tables

Figures

◀

▶

◀

▶

Back

Close

Full Screen / Esc

Printer-friendly Version

Interactive Discussion



Transport pathways
of peroxyacetyl
nitrate

S. Fadnavis et al.

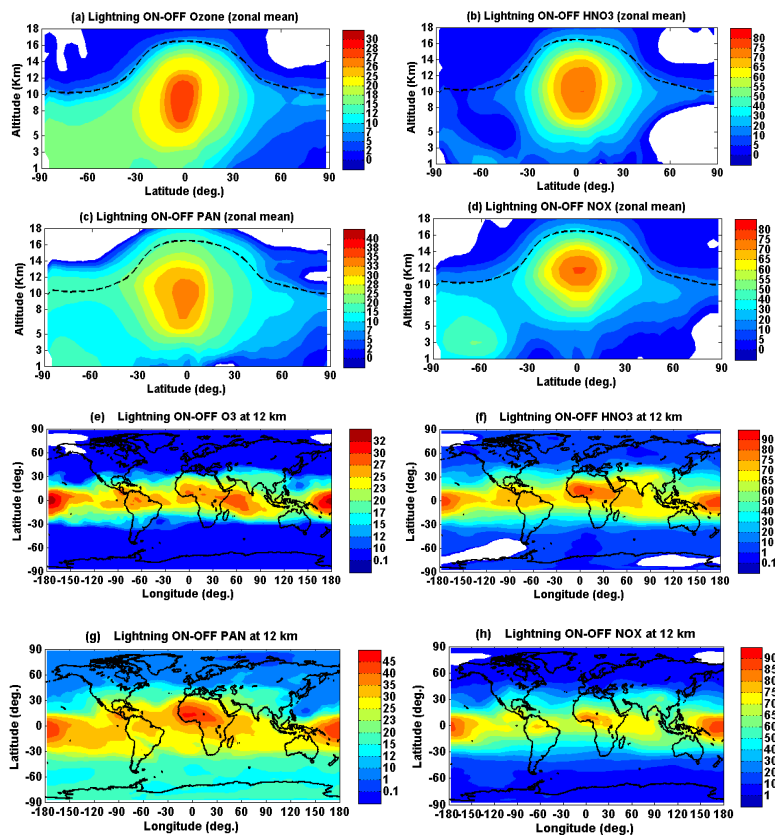


Figure 10. Zonal averaged seasonal mean changes (percentage) produced from lightning in (a) ozone (b) HNO₃ (c) PAN (d) NO_x, distribution of seasonal mean changes (percentage) produced from lightning in (e) ozone (f) HNO₃ (g) PAN (h) NO_x at 12 km.

Title Page

Abstract

Introduction

Conclusions

References

Tables

Figures



Back

Close

Full Screen / Esc

Printer-friendly Version

Interactive Discussion

